AGU PUBLICATIONS

JGR

Journal of Geophysical Research: Solid Earth

RESEARCH ARTICLE
10.1002/2016JB013858

This article is a companion to *Tadini et al.* [2017] doi:10.1002/2016JB013860.

Key Points:
- A new geodatabase for Somma-Vesuvio eruptions and structures is presented with >1700 elements stored in 14 feature classes grouped in five data sets
- Innovative characterizations of spatial uncertainty areas for each feature are introduced as key new geodatabase information elements
- The new database is used in a companion paper to develop the first spatial probability vent opening map for the Somma-Vesuvio caldera

Supporting Information:
- Supporting Information S1
- Data Set S1
- Table S1
- Table S2
- Table S3

Correspondence to:
A. Tadini,
alessandro.tadini@ingv.it

Citation:
Tadini, A., M. Bisson, A. Neri, R. Cioni, A. Bevilacqua and W. P. Aspinall (2017), Assessing future vent opening locations at the Somma-Vesuvio volcanic complex: 1. A new information geodatabase with uncertainty characterizations, *J. Geophys. Res. Solid Earth*, *122*, doi:10.1002/2016JB013858.

Received 14 DEC 2016
Accepted 13 APR 2017
Accepted article online 4 MAY 2017

Assessing future vent opening locations at the Somma-Vesuvio volcanic complex: 1. A new information geodatabase with uncertainty characterizations

A. Tadini[1,2], M. Bisson[2], A. Neri[2], R. Cioni[1], A. Bevilacqua[2,3,4], and W. P. Aspinall[5,6]

[1]Dipartimento di Scienze della Terra, Università di Firenze, Florence, Italy, [2]Sezione di Pisa, Istituto Nazionale di Geofisica e Vulcanologia, Pisa, Italy, [3]Scuola Normale Superiore, Pisa, Italy, [4]Now at Department of Geology, State University of New York at Buffalo, Buffalo, New York, USA, [5]Aspinall and Associates, Tisbury, UK, [6]School of Earth Sciences and Cabot Institute, University of Bristol, Bristol, UK

Abstract This study presents new and revised data sets about the spatial distribution of past volcanic vents, eruptive fissures, and regional/local structures of the Somma-Vesuvio volcanic system (Italy). The innovative features of the study are the identification and quantification of important sources of uncertainty affecting interpretations of the data sets. In this regard, the spatial uncertainty of each feature is modeled by an uncertainty area, i.e., a geometric element typically represented by a polygon drawn around points or lines. The new data sets have been assembled as an updatable geodatabase that integrates and complements existing databases for Somma-Vesuvio. The data are organized into 4 data sets and stored as 11 feature classes (points and lines for feature locations and polygons for the associated uncertainty areas), totaling more than 1700 elements. More specifically, volcanic vent and eruptive fissure elements are subdivided into feature classes according to their associated eruptive styles: (i) Plinian and sub-Plinian eruptions (i.e., large- or medium-scale explosive activity); (ii) violent Strombolian and continuous ash emission eruptions (i.e., small-scale explosive activity); and (iii) effusive eruptions (including eruptions from both parasitic vents and eruptive fissures). Regional and local structures (i.e., deep faults) are represented as linear feature classes. To support interpretation of the eruption data, additional data sets are provided for Somma-Vesuvio geological units and caldera morphological features. In the companion paper, the data presented here, and the associated uncertainties, are used to develop a first vent opening probability map for the Somma-Vesuvio caldera, with specific attention focused on large or medium explosive events.

1. Introduction

Somma-Vesuvio (SV) is one of the most dangerous volcanoes in the world. Its surroundings are very densely inhabited with more than 600,000 people living within 6 km of the present crater, on top of Gran Cono. Moreover, SV eruptive styles are significantly variable, ranging from relatively gentle lava effusions to devastating Plinian eruptions [*Cioni et al.*, 2008].

In the last few decades, many studies have been carried out on SV with a variety of aims such as reconstructing and classifying its eruptive history [e.g., *Principe et al.*, 2004; *Cioni et al.*, 2008], characterizing the composition of its eruptive products [*Santacroce et al.*, 2008, and references therein], describing the distributions of geological and morphological features [*Santacroce and Sbrana*, 2003; *Ventura et al.*, 2005; *Vilardo et al.*, 2009; *Gurioli et al.*, 2010; *Principe et al.*, 2013], and recording activity from geophysical and geochemical monitoring [*Vilardo et al.*, 1996; *Scarpa et al.*, 2002; *Aiuppa et al.*, 2004; *Federico et al.*, 2004; *Frondini et al.*, 2004; *De Natale et al.*, 2006; *Cella et al.*, 2007; *De Siena et al.*, 2009; *Granieri et al.*, 2013].

The work presented here complements available volcanological information with new and revised data sets and with elaborations that address specifically the locations of the vents of past eruptions and eruptive fissures, as well as other structural features. The reconstruction of previous activity of SV highlights the significant past variability in vent locations of both explosive [*Cioni et al.*, 2008, and references therein] and effusive [*Nazzaro*, 1997; *Ricciardi*, 2009] activities. Such variability had a notable influence on the distribution of eruptive products around the volcano, particularly those associated with the emplacement of pyroclastic density currents. Clear evidence for the influence of spatial source effects is found in the mapped deposits [*Gurioli et al.*, 2010] and shown as well by outcomes of 3-D simulations of column-collapse scenarios at SV [*Esposti Ongaro et al.*, 2008a, 2008b].

A key feature of the present study is the inclusion of information about the uncertainties affecting the data sets. Particular attention is given to the definition of the spatial uncertainties associated with the locations of vents and fissures. Such uncertainties can be substantial for the oldest and bigger explosive events, given the largely incomplete reconstruction of volcanic deposits (particularly in the most proximal localities and in distal areas) and to the uncertainty related to possible shifts of vent location during a single event. In some cases, uncertainty bounds for specific features were also estimated by critically comparing and integrating data derived from different sources (for instance, for the location of effusive vents) or by accounting for the accuracy of the methods used to obtain them (in the case of structural data). A similar approach was followed by *Bevilacqua et al.* [2015] for the characterization of the uncertainty of past vent locations and structural features at Campi Flegrei caldera (Italy).

The new data sets are organized into an updatable geodatabase adopting a geographically referenced framework. The database utilizes geographic information system (GIS) methodology based on the Environmental Systems Research Institute platform [*Mitchell*, 1999] for data storage and representation, although the data sets are also readable with different GIS platforms. This new database integrates and complements existing databases of SV, such as that of *Vilardo et al.* [2009] that includes, on a webGIS platform, geographical, territorial, morphological, and geophysical data (raster and vector), as well as seismicity catalogues (http://ipf.ov.ingv.it/siscam.html).

The quantification of the different sources of uncertainty affecting the data sets is a crucial step for volcanological studies, particularly for those aimed at the assessment of volcanic hazard and risk mitigation. A first application of the new data sets presented here is described by *Tadini et al.* [2017], where a vent opening probability map for SV has been produced for the first time with specific reference to the occurrence of large or medium explosive events.

In the following sections a summary of the tectonic setting and eruptive history of SV is given (section 2), followed by a brief technical description of the geodatabase (section 3), a description of the main sources of uncertainty and their quantification (section 4) and the presentation of the new and revised data sets (section 5). Finally, section 6 briefly concludes with a few remarks about potential uses and applications of the new geodatabase.

2. Geological Setting of Somma-Vesuvio

2.1. Tectonic Setting

The SV volcanic complex lies in the Campanian plain (Figure 1a), a structural depression of Plio-Quaternary age filled with marine, continental, and volcanic sediments of early Pleistocene–Holocene age [e.g., *Santangelo et al.*, 2010, and references therein].

Crustal thickness varies between 25 km in the Phlegrean Fields area and 35 km in the SV area [*Locardi and Nicolich*, 1988; *Ferrucci et al.*, 1989]. Gravimetric data [*Finetti and Morelli*, 1974; *Berrino et al.*, 1998] suggest that in the Vesuvian area the sedimentary basement is about 11 km thick, with the top at a depth of 2 km, as also confirmed by the results of the geothermal drilling Trecase 1, on the southern lower slopes of the volcano [*Cassano and La Torre*, 1987].

Tectonic structures affecting the Campanian plain consist of NW-SE/NNW-SSE and NNE-SSW/NE-SW trending faults with normal to sinistral movements for the NW-SE trending faults and normal to dextral for the NE-SW trending structures (Figure 1b), in agreement with the NNE-SSW orientation of the σ_{Hmin} axis of the regional stress field [*Hippolyte et al.*, 1994; *Bianco et al.*, 1998]. The regional stress field which developed the above-mentioned normal to strike-slip faults was active during early Pleistocene, with an ENE-WSW direction of compression [*Hippolyte et al.*, 1994]. The same authors indicate a present, regional σ_{Hmin} with an NE-SW strike: these data are furthermore confirmed by a single analysis (Figure 1a) from World Stress Map Data [*Heidbach et al.*, 2008], which indicate an N76° strike for σ_{Hmin}. E-W faults with normal component of movement are also recognized in the area of the SV caldera [*Bianco et al.*, 1998].

Movements of faults in the SV area are mostly related to the regional stress field, although a local stress field (ESE-WNW trending σ_{Hmin}) has been demonstrated for second-order movements of faults [*Bianco et al.*, 1998]. Shear wave splitting analysis performed at SV revealed that NW-SE discontinuities (faults and fractures)

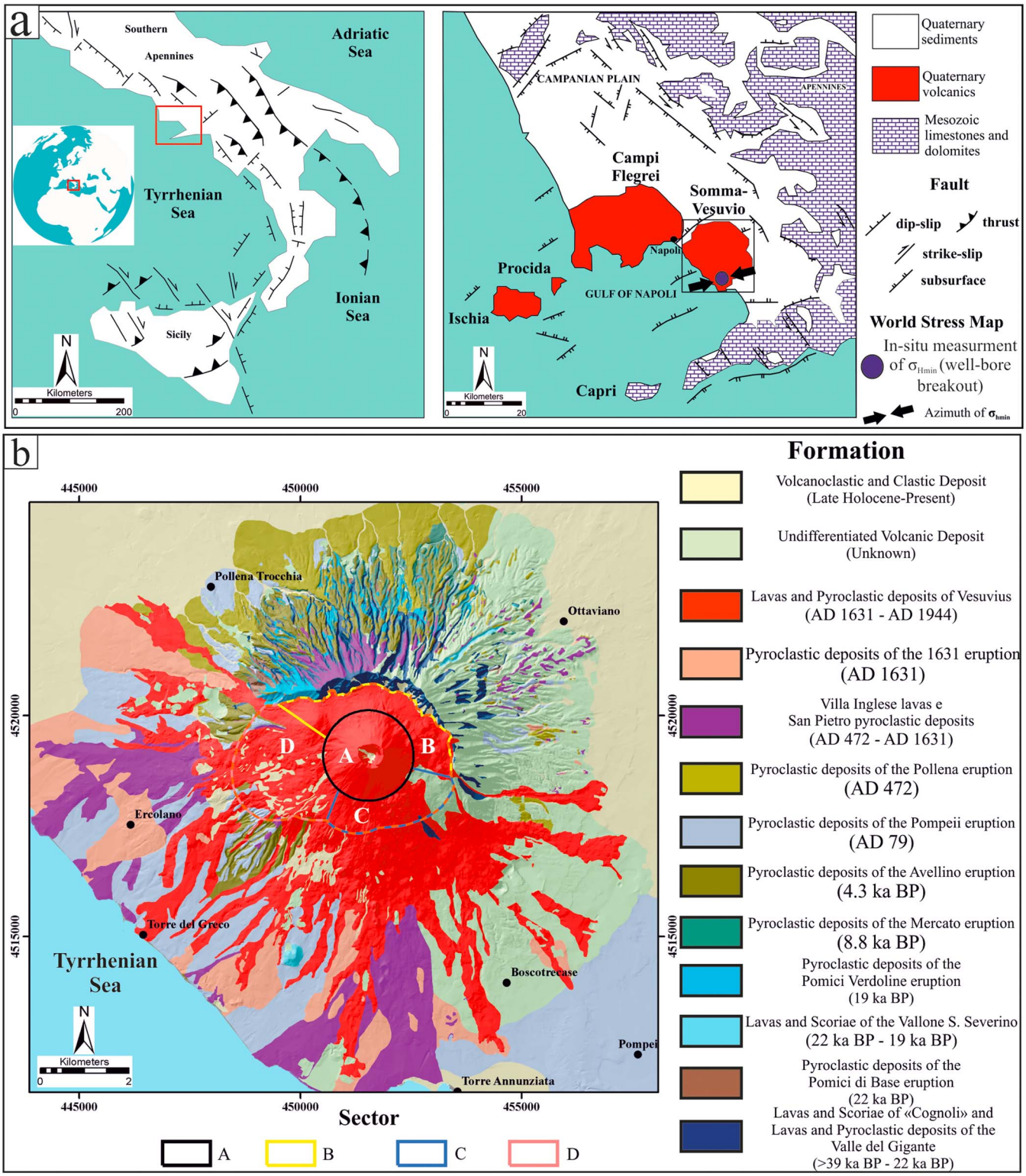

Figure 1. Morphostructural sketch and geological units of the Somma-Vesuvio (SV) region. (a) Morphostructural sketch of southern Italy and Campanian plain with the most important tectonic features highlighted and World Stress Map data [*Bianco et al.*, 1998; *Heidbach et al.*, 2008]; (b) geological units of SV volcanic complex [*Santacroce and Sbrana*, 2003]. SV caldera (outlined in dark orange dashed line) and caldera sectors are defined in subsection 5.1.

might extend down to at least 6 km depth and may thus represent the main group of structural discontinuities that affect the volcano [*Bianco et al.*, 1998].

The asymmetric shape of the western slope of SV has been interpreted by *Ventura et al.* [1999] and *Milia et al.* [2007, 2012] to be the consequence of several flank failures that occurred in association with major Plinian eruptions. Such failures could have eventually modified the shallow plumbing system of SV, inducing the shift from prevalent effusive activity of Mount Somma to a more explosive nature, starting about 22 ka ago with the oldest Plinian eruption of SV ("Pomici di Base" Plinian eruption) [*Ventura et al.*, 1999]. However, recent stratigraphic data from a borehole drilled SW of the SV volcanic edifice [*Di Renzo et al.*, 2007] exclude the presence of debris avalanche deposits related to flank collapses, at least in the last 20 ka, while *Sulpizio et al.* [2008] rebutted the interpretations of *Ventura et al.* [1999] and *Milia et al.* [2007] on the grounds of stratigraphic inconsistencies between the suggested age of collapses and the primary deposits still present within the inferred collapsed area.

2.2. Eruptive History

The SV is a composite volcano with an old edifice (Mount Somma) dissected by multiple summit caldera collapses [*Cioni et al.*, 1999]. A stratocone grew discontinuously inside the summit caldera after the A.D. 79 Pompeii Plinian eruption, and the present cone (Vesuvio or Gran Cono) is related to the activity after the A. D. 1631 sub-Plinian I eruption. SV activity has been reconstructed in several papers, including *Cioni et al.* [2008], who also suggested the classification scheme used in the following discussion.

The present edifice of SV started to be formed after the Campanian Ignimbrite eruption of Campi Flegrei (39 ka B.P.) and continued up to A.D. 1944, with periods of quiescence alternating with periods of intense explosive and effusive activity. The eruption of 1944 marked the transition from an "open conduit" condition, which characterized the activity of SV in the period 1631–1944, to an obstructed conduit state. Recent tomographic investigations of the SV substratum [*Auger et al.*, 2001; *Iuliano et al.*, 2002; *Scarpa et al.*, 2002; *Zollo et al.*, 2002; *Del Pezzo et al.*, 2006] indicate that (a) evidence exists for a high-velocity anomaly below the crater area; (b) a large magma body (volume bigger than 0.1–0.2 km^3) within the shallowest 8 km of depth can be discounted; and (c) a regionally wide magma reservoir at a depth of 8–10 km is suggested.

Mount Somma activity (from 39 up to 22 ka B.P.) has been prevalently effusive, producing a thick lava pile interbedded with spatter and cinder deposits (Figure 1b). Conversely, starting from the Pomici di Base eruption (22 ka B.P.; Figure 1b), at least four high-magnitude Plinian eruptions occurred (i.e., Pomici di Base, Mercato, Avellino, and Pompeii), interspersed by three major sub-Plinian I eruptions (Greenish Pumices, A. D. 472 Pollena and A.D. 1631), three minor sub-Plinian II eruptions (AP1, AP2, and A.D. 512), and several minor events, characterized by a quite large range of magnitudes and intensities, falling in the categories of violent Strombolian and continuous ash emission eruptions (see *Cioni et al.* [2008] for further details).

Plinian eruptions at SV approximately range in magnitude between 1 and 5 km^3 of deposits and in intensity between 10^7 and 10^8 kg/s. They are characterized by widely dispersed fallout tephra sheets (up to 2000 km^2 covered by 10 cm of deposit) [*Cioni et al.*, 2008] and large thicknesses (up to 35 m) of pyroclastic density current (PDC) deposits dispersed up to a maximum distance of about 15 km [*Gurioli et al.*, 2010]. Each of the four Plinian eruptions resulted in a caldera collapse that contributed to the present asymmetric shape of the SV polyphased caldera [*Cioni et al.*, 1999].

Sub-Plinian I eruptions approximately range in magnitude between 0.1 and 1 km^3, with intensities of 10^7 kg/s as order of magnitude. Similar in character to Plinian eruptions, they have dispersed tephra fallout sheets (up to 1000 km^2 covered by 10 cm of deposit) and thick PDC deposits (up to 20 m), spread up to a maximum distance of about 8–10 km from the vent [*Gurioli et al.*, 2010]. Plinian and sub-Plinian I PDC deposits crop out in the different sectors of the edifice and its apron (Figure 1b), showing variable dependence on preexisting topography [*Santacroce and Sbrana*, 2003]. Only the PDC deposits of the 1631 sub-Plinian I eruption do not crop out along the northern sector of Mt. Somma.

Sub-Plinian II eruptions (AP1, AP2, and A.D. 512) range in magnitude between 10^{-2} and 10^{-1} km^3 and in intensity between 10^6 and 10^7 kg/s [*Andronico and Cioni*, 2002; *Cioni et al.*, 2011]. Relatively small tephra sheets (less than 400 km^2 covered by 10 cm of deposit) and very minor PDC beds dispersed within 2–3 km from the vent represent the deposits from these eruptions.

Table 1. Mean Values of the Age, Volume, and Intensity as Estimated for Plinian (Pl), Sub-Plinian (Spl1 and Spl2), and Violent Strombolian (VS) to Continuos Ash Emission (AE) Eruptions (From *Cioni et al.* [2008])[a]

					Caldera Sector			
Eruption	Type	Age	Volume (Deposit, km^3)	Intensity (kg/s)	A	B	C	D
Pomici di Base	Pl	22.0 ka B.P.	4.40	2.5×10^7	34.1%	9.7%	5.0%	51.2%
Greenish Pumices	Spl1	19.2 ka B.P.	0.50	1.7×10^7	32.2%	22.6%	0%	45.2%
Mercato	Pl	8.8 ka B.P.	1.83	2.8×10^7	50.5%	20.0%	18.5%	11.0%
Avellino	Pl	4.3 ka B.P.	0.41	1.1×10^8	0%	0%	0%	100%
AP1	Spl2	3.2 ka B.P.	0.147	–	0%	0%	0%	100%
AP2	Spl2	3.0 ka B.P.	0.143	1.0×10^7	0%	0%	0%	100%
AP3	AE	2.7 ka B.P.	0.15	3.0×10^6	100%	0%	0%	0%
AP4	VS-AE	?	0.122	–	100%	0%	0%	0%
AP5	VS-AE	?	0.084	–	100%	0%	0%	0%
Pompeii	Pl	A.D. 79	1.05	1.1×10^8	39.6%	25.4%	27.1%	7.9%
S. Maria cycle	VS-AE	A.D. 172–A.D. 305	0.15	–	100%	0%	0%	0%
Pollena	Spl1	A.D. 472	0.42	2.0×10^7	36.4%	47.2%	0%	16.4%
A.D. 512	Spl2	A.D. 512	0.09	2.0×10^6	100%	0%	0%	0%
AS2	VS	A.D. 547	0.04	4.0×10^6	100%	0%	0%	0%
AS3	VS	A.D. 707	0.12	–	100%	0%	0%	0%
AS4	VS	A.D. 857	0.01	–	100%	0%	0%	0%
A.D. 1631	Spl1	A.D. 1631	0.46	4.7×10^7	100%	0%	0%	0%
A.D. 1682	VS	A.D. 1682	0.0056	8.0×10^3	100%	0%	0%	0%
A.D. 1707	VS	A.D. 1707	0.0013	6.0×10^3	100%	0%	0%	0%
A.D. 1723	VS	A.D. 1723	0.008	2.0×10^4	100%	0%	0%	0%
A.D. 1730	VS	A.D. 1730	0.0012	3.8×10^5	100%	0%	0%	0%
A.D. 1779	VS	A.D. 1779	0.0061	3.4×10^5	100%	0%	0%	0%
A.D. 1822	VS	A.D. 1822	0.038	3.8×10^6	100%	0%	0%	0%
A.D. 1906	VS	A.D. 1906	0.071	2.8×10^6	100%	0%	0%	0%
A.D. 1944	VS	A.D. 1944	0.066	9.5×10^5	100%	0%	0%	0%

[a]Values in the "Caldera Sector" column refer to the percentage of the vent location uncertainty areas (see the definition in section 4) for each eruption that belongs to each of the caldera sectors defined in Figure 1.

Violent Strombolian (VS) eruptions, with approximate magnitudes of 10^{-3} to 10^{-2} km^3 and intensities of 10^5 to 10^6 kg/s, are associated with lapilli and ash fallout deposition and minor avalanching of hot materials, mainly confined to the slopes of the cone (e.g., 1822 and 1944 eruptions). Continuous ash emission (AE) eruptions (e.g., AP3, AP4, and AP5, several events of Middle Age activity, 1794, and 1660)—with magnitudes up to 10^{-2} km^3 and intensities $<10^5$ kg/s—resulted in the deposition of sequences (from few centimeters up to several decimeters thick) of ash deposits interlayered with minor lapilli beds. The most important feature of this latter type of activity is its prolonged duration (from weeks to months) (details in *Cioni et al.* [2008] and *Barsotti et al.* [2015]).

Cioni et al. [2008] discussed in detail the temporal evolution of volcanic activity at SV, by estimating the main physical parameters related to a large set of past eruptions (see Figure 3 from this paper and Table 1 from *Cioni et al.* [2008]). Age, erupted volume, and intensity of Plinian, sub-Plinian, and violent Strombolian to continuous ash emission eruptions have been summarized in Table 1, and the vent location uncertainty area of each eruption defined in this paper (see section 4) has been associated with the different caldera sectors (see Figure 1 and section 3 for sector definition). As a general observation, the time span between two successive Plinian eruptions (i.e., inter-Plinian periods) decreased with time; conversely (based on the available data, which might suffer some under-reporting of lower magnitude eruptions), activity became more and more frequent starting from at least about 4 ka (following the Avellino Pumice eruption), while generally decreasing in intensity [*Cioni et al.*, 2008]. Vent positions are mostly concentrated in three of four caldera sectors (Sectors A, B and D; see Figure 1b), without any clear trend of a shift in vent positions with time. Whereas the vent position of the four Plinian eruptions invariably changed from one Plinian eruption to the next, a few sub-Plinian eruptions possibly may have shared the same vent position as the immediately preceding Plinian event (e.g., AP1 and AP2 eruptions issued from the same vent area as the Avellino Pumice eruption; the A.D. 512 and A.D. 1631 eruptions were from the same vent area as the Pompeii Pumice). Finally, only low-magnitude (and low-intensity) eruptions issued from vents outside the present caldera.

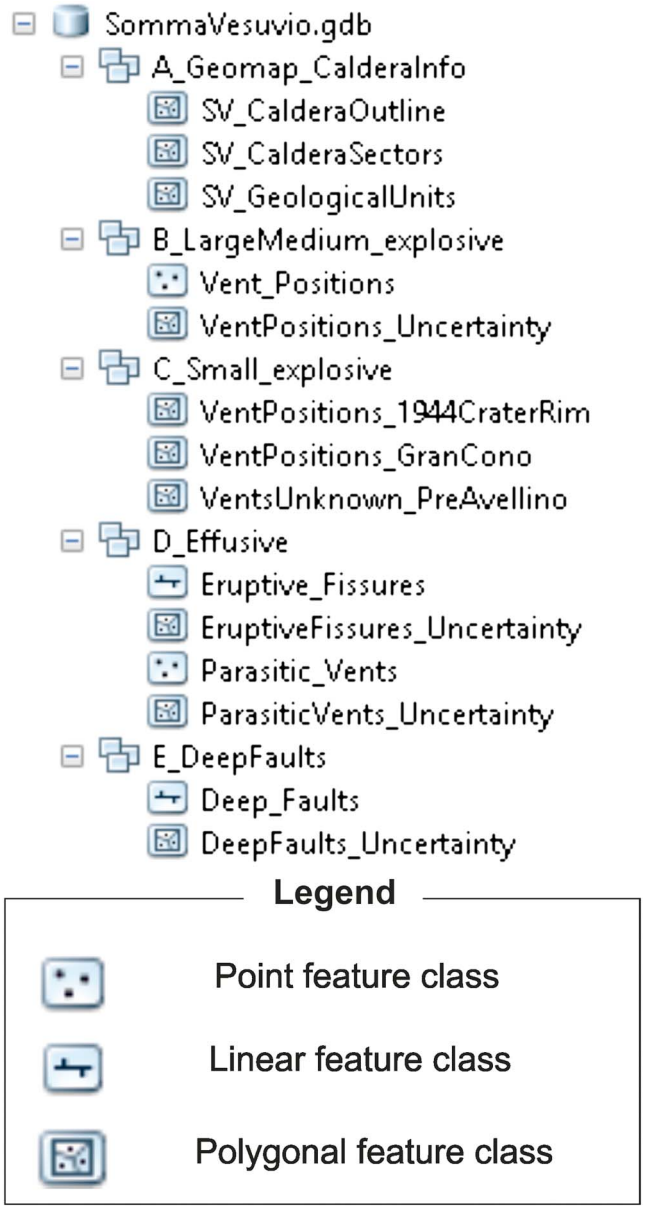

Figure 2. Structure of the SV geodatabase. Data set contents are described and discussed in section 5 of the main text. The geodatabase is available in this format in Data Set S1.

Effusive activity at SV, except for the Mount Somma lavas, apparently has been mostly limited to the last 1000 years of activity, following the eruption of A.D. 472 [*Arrighi et al.*, 2001; *Cioni et al.*, 2008; *Scandone et al.*, 2008]. Effusive activity could have occurred also during other inter-Plinian periods, confined to the progressively enlarged and deepened caldera structure. During the period of semipersistent activity between 1639 and 1944, a total of 99 eruptions occurred (sometimes predominantly effusive but very often accompanied with Strombolian to violent Strombolian activity), each separated by an average quiescence of 3–4 years, but none exceeding 7 years [*Arrighi et al.*, 2001; *Scandone et al.*, 2008]. Other periods of mild Strombolian to effusive activity occurred between the Pompeii Plinian eruption and the A.D. 472 sub-Plinian I eruption (S. Maria cycle [*Principe et al.* [2004]) and discontinuously after the A.D. 512 sub-Plinian II eruption up to A.D. 1139 [*Cioni et al.*, 2008; *Scandone et al.*, 2008].

For a complete review of the compositional features of SV volcanic products, which is beyond the scope of this study, see *Santacroce et al.* [2008, and references therein].

3. The Geodatabase and Its Properties

For the development of the geodatabase presented here, we have adopted the ArcGIS 10.1® geodatabase platform since it is a repository that offers efficient storage and logical organization of spatial data.

The geodatabase of SV contains more than 1700 elements stored in 11 feature classes (point, linear, and polygonal) and grouped as four main data sets dealing with volcanological (vent position and related uncertainty) and structural information. Polygonal feature classes represent the spatial uncertainty areas of the related data, which are represented through point or linear feature classes. An additional data set stores information about geological mapping (one feature class) and caldera structure (two feature classes). In total, the geodatabase (Figure 2) therefore comprises 14 feature classes grouped in 5 data sets, as follows: (i) geological mapping and caldera information (see subsection 5.1); this data set records the spatial distribution of volcanic products as displayed in the latest geological map of SV [*Santacroce and Sbrana*, 2003] along with geomorphological data about the SV caldera outline and SV caldera sectors; (ii) a data set recording the spatial distribution of vents associated with large- or medium-scale explosive activity (i.e., Plinian and sub-Plinian I and II eruptions, see subsection 5.2); (iii) a data set recording the spatial distribution of vents associated

with small-scale explosive activity (i.e., violent Strombolian to continuous ash emission eruptions, see sub section 5.3); (iv) a data set recording the spatial distribution of volcanic features associated with effusive activity (i.e., parasitic vents and eruptive fissures, see subsection 5.4) and subdivided into parasitic vent and eruptive fissure subdata sets; (v) and a data set containing spatial information on regional/local structures and locations of deep faults (see subsection 5.5).

All the data presented in the following sections have been imported into the geodatabase and geocoded to WGS84 UTM ZONE 33 coordinate system. A 10 m cell size digital elevation model [*Tarquini et al.*, 2007] is used as the reference topographic base for data set visualizations.

4. Uncertainty Description and Quantification

The design of the new geodatabase is based on the assimilation of vector data, organized so that it can be queried. The vector data are obtained by transforming—into digital format—information from bibliographic sources, direct measurements, and field surveys. As several sources of uncertainty can affect the final quality of data, evaluating their accuracy (in our case, the uncertainty in feature locations) is not straightforward. Sources of errors and uncertainties can be due to many factors, including the intrinsic variability of any natural process and others that are related to data operations (e.g., data acquisition during field work, instrumental precision, and transformation of analogue data to digital).

In many hazard assessment studies, these factors are differentiated into two classes of uncertainty: epistemic (i.e., knowledge-related, potentially reducible by acquiring more or better information) and aleatoric (inherent randomness, also called physical variability). While both types are relevant to event forecasting [see, for example, *Aspinall*, 2006; *Bevilacqua*, 2016; *Bevilacqua et al.*, 2015, 2016; *Marzocchi and Bebbington*, 2012; *Neri et al.*, 2008, 2015; *Sparks and Aspinall*, 2004; *Woo*, 1999], their numerical treatments differ within a probabilistic analysis, and definitions and attributions need care.

A full discussion of these issues is beyond the scope of this study, which instead focuses on the quantitative representation of the uncertainty related to our knowledge of vent location of past events and of the main structural features possibly controlling vent opening. Such sources of uncertainty can be significant and, as mentioned above, ideally should be properly accounted for [e.g., *Matthies*, 2007].

In our specific case study, uncertainty can arise due to possible ambiguity in field observations, measurements or other data errors, and from paucity or lack of empirical elements that help to constrain the reconstruction of precise positions of volcanological and structural features. For instance, when dealing with vent locations, the position of a past vent is typically inferred by reconstructing the spatial patterns of different deposits (fallout isopachs, distribution of pyroclastic density current deposits, venting area of lava flows, etc.). However, as is evident, isopach reconstruction introduces a subjective degree of interpretation (and thus an uncertainty) that generally decreases with the number of suitable outcrops where thickness of proximal fall deposits can be measured [*Engwell et al.*, 2015]. Added to this, an absence of very proximal outcrops, close to an originating vent, precludes the vent area from being precisely delineated, further increasing the uncertainty. In consequence, uncertainties are greater for older eruptions where such diagnostic deposits have been eroded, partially covered by younger deposits or affected by recent urbanization (particularly dense in the Somma-Vesuvio area), or where the area close to the vent has been deeply modified by subsequent volcanic activity.

In relation to vent areas, and especially for Plinian events, the temporal evolution of the process was also accounted for. In these cases, intrinsic complexities of the dynamics of the eruption, such as possible vent migration during the event, or the simultaneous activity of multiple vents or eruptive fissures produced by caldera collapse, can significantly enlarge such areas of uncertainty. Given the inevitable uncertainties in relation to past events, it is very difficult, if not impossible, to distinguish between physical variability and spatial uncertainty, so these have had to be considered jointly in our assessment of uncertainty of vent location, as described in the following sections.

Besides these sources of uncertainty, for some of the data sets, we have also considered other uncertainties which are related to possible misinterpretation of available data (e.g., uncertainties in the location of presumed effusive parasitic vents) or resolution limits of field data (e.g., uncertainty in the location of deep faults or of buried parasitic vents, when position is determined from interpretation of seismic reflection profiles).

The uncertainty areas, built around the features, are drawn differently according to feature geometry. The sizes and shapes of uncertainty areas were defined on the basis from the available data and specific knowledge of the SV complex. As is discussed in more detail in the companion paper [*Tadini et al.*, 2017], it is assumed that such uncertainty areas enclose 100% probability of feature location and that for the sake of simplicity, such probability is uniformly distributed over the uncertainty area. In general, in the case of a point feature, the uncertainty area is proscribed as a circle or a polygon centered on the feature itself, with a radius representing the spatial uncertainty associated with the point position. For linear features, in contrast, the uncertainty area is a polygon that can be drawn by putting its boundaries at a constant distance from the line itself. The width of the polygon represents the spatial uncertainty related to the line position. In the present study of SV, we define uncertainty areas with a variable radius (and shape) for large- or medium-scale explosive eruptions, small-scale explosive eruptions, and for the eruptive fissures. For representing the uncertainty areas of parasitic vents, we use a circular area with fixed radius and, to represent the uncertainty in the location of deep faults, a rectangular buffer area with fixed width.

At this stage, uncertainty areas with uniform 100% probability density inside were fixed by the authors without the use of structured expert elicitation techniques [e.g., *Cooke*, 1991; *Aspinall*, 2006]; the same basic assumption was adopted by *Bevilacqua et al.* [2015] in a similar study on Campi Flegrei caldera and was considered appropriate also for the aims of this study.

5. The Data Sets

5.1. Geological Mapping and Caldera Information

Geological mapping and caldera morphological features are included in the geodatabase with the specific aim of facilitating the characterization of the other volcanological data sets and of helping in their interpretation and elaboration [see also *Tadini et al.*, 2017].

Geological units from the latest geological map of SV [*Santacroce and Sbrana*, 2003] were digitized and included in the geodatabase to integrate volcanological, structural, and geological data, particularly for the attribution of a given period of activity to parasitic vents and eruptive fissure ages. A simplified version of such feature classes, where different formations have been grouped into major units representing specific temporal intervals of SV activity or specific type of deposits, is shown in Figure 1b. Geological units have been stored in a polygonal feature class where each record is classified according to the information provided in the geological map (formation, code of formation, type of deposit, age, and labels). A total of 13 formations for primary volcanic deposits (lava flows, PDC deposits, and fallout deposits) and two formations for alluvial and clastic/volcanoclastic deposits comprise the feature class. Deposits cover the whole volcanic history of SV, starting from Mount Somma activity ("Lave e Piroclastiti della Valle del Gigante" and "Lave e Scorie dei Cognoli"; Figure 1b) through the more recent activity of the volcano ("Lave e Piroclastiti del Vesuvio"; Figure 1b).

The SV caldera morphological outline and a simplified morphological partitioning of it are also included in the geodatabase as two other polygonal feature classes. The present SV caldera outline (Figure 1b and following figures) has been drawn by taking into consideration morphological limits (the foot of Mount Somma northern scarp) and the caldera collapse extent of Plinian eruptions based on other morphological features (sharp changes in the slope, evidences from the hydrographic network, etc. [*Cioni et al.*, 1999]) and is represented through a polygonal feature class. The surface area enclosed by this caldera outline is 12.98 km^2.

To provide more information about parasitic vents and eruptive fissure location (see sections 5.4.1 and 5.4.2), as well as to facilitate considerations about the potential areas of vent openings [*Tadini et al.*, 2017], the SV caldera has been subdivided into four sectors (labelled A, B, C, and D), whose definitions are mostly related to the morphological features of the SV caldera (Figure 1b). In detail, sector A encloses the present area of Gran Cono and is bordered by the break in slope at the base of the cone; sector B refers to the N-NE part of SV caldera (delineated by the Mount Somma scarp) and approximately corresponds to the "Valle del Gigante" area; sector C encloses the SE part of the SV caldera and approximately corresponds to the "Valle dell'Inferno" area; and sector D refers to the W part of SV caldera and includes the "Piano delle Ginestre" area. The areal size of the four sectors varies between about 2.1 km^2 for sector C up and about 4 km^2 for sector D.

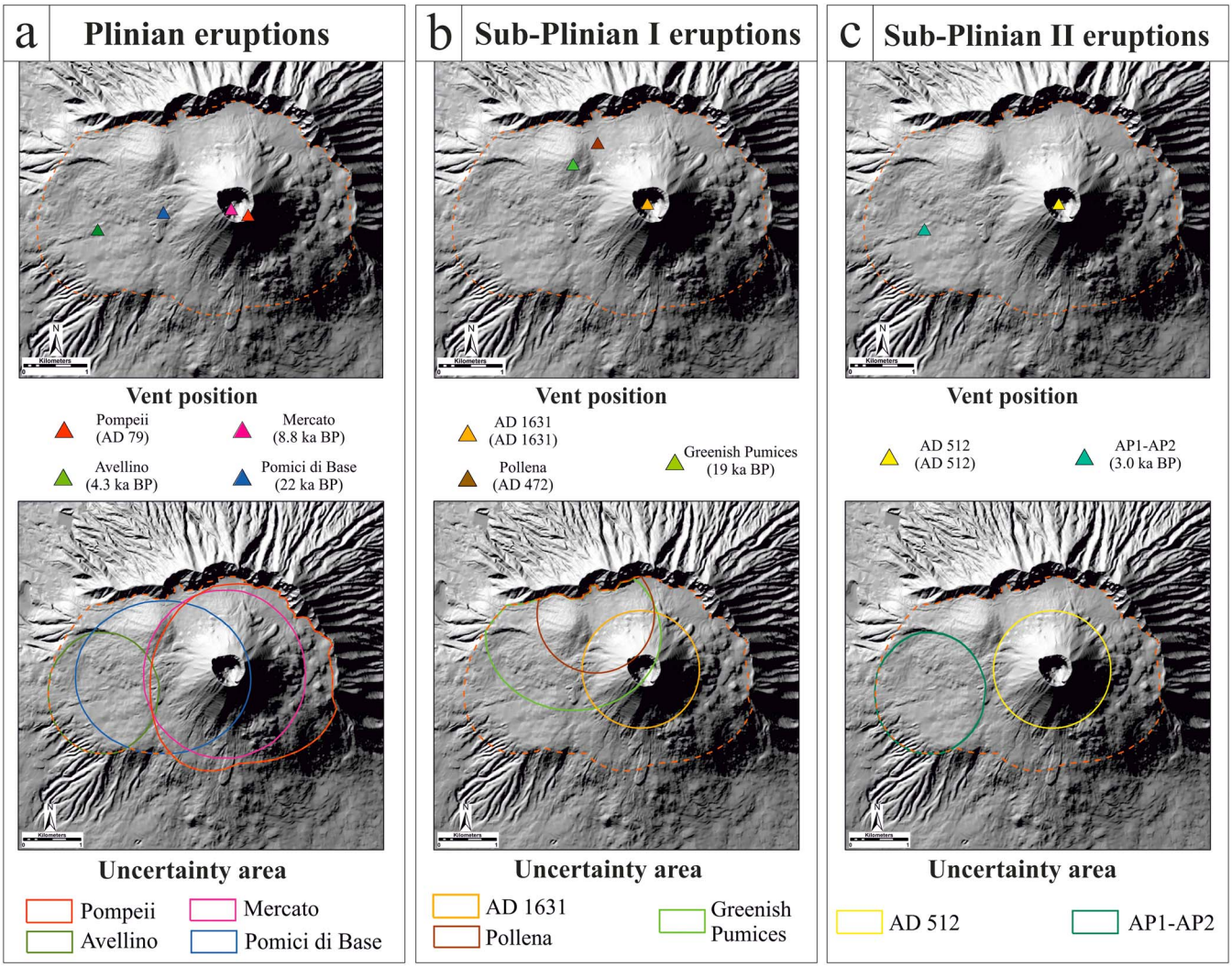

Figure 3. Large- or medium-scale explosive eruption data set. The data set includes (a) four Plinian eruptions, (b) three sub-Plinian I eruptions, and (c) three sub-Plinian II eruptions. Each group of eruptions comprises a feature class indicating the vent positions as a point (from *Gurioli et al.* [2010]) and a feature class representing the associated spatial uncertainty area. SV caldera is outlined in dark orange dashed line.

5.2. Vent Location of Large- or Medium-Scale Explosive Eruptions

The data set of large or medium explosive eruptions groups two feature classes that account for the vent positions and their associated uncertainty areas (Figure 3) related to four Plinian, three sub-Plinian I, and three sub-Plinian II events, according to the classification introduced by *Cioni et al.* [2008].

For Plinian eruptions (Figure 3a), uncertainty areas are taken to be equal to the area of the associated caldera collapse, as defined in *Cioni et al.* [1999]. Despite the available data related to fallout isopachs [*Bertagnini et al.*, 1998; *Cioni et al.*, 2000; *Gurioli et al.*, 2005; *Gurioli et al.*, 2010; *Mele et al.*, 2011] that help to constrain possible vent positions for these eruptions, there are wide uncertainties associated with them, also due to possible vent migration during each Plinian eruption (e.g., following caldera collapse). For these Plinian events, dimensions and shapes of uncertainty areas are linked to the accuracy of morphological constraints used by *Cioni et al.* [1999] to delineate the collapsed areas. As a result, the Pompeii and Avellino eruptions have uncertainty areas that are better defined than the older Mercato and Pomici di Base eruptions, which have fewer morphological constraints [see *Cioni et al.*, 1999].

Data from fallout isopachs [*Rosi et al.*, 1993; *Cioni et al.*, 2003; *Sulpizio et al.*, 2005] allowed *Gurioli et al.* [2010] to display inferred vent locations also for sub-Plinian I eruptions (Figure 3b). We define uncertainty areas associated with vent locations in a way similar to that for Plinian eruptions. The definition

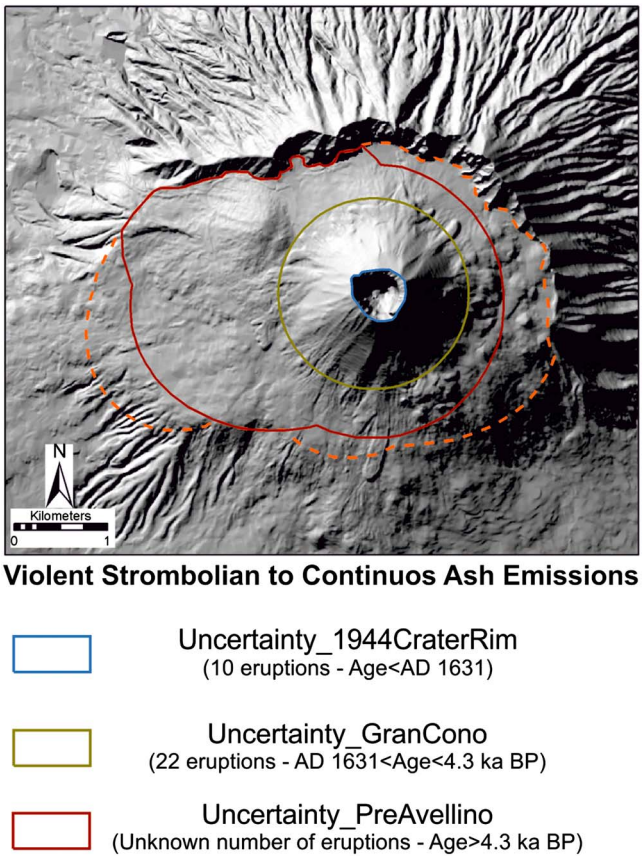

Figure 4. Small-scale explosive eruption data set. The data set includes 32 eruptions whose vents are distributed over three uncertainty areas: (1) the area included within the 1944 crater rim, where 10 eruptions occurred since the A.D. 1631 sub-Plinian event; (2) the area of Gran Cono, where in the period between the Avellino (4.3 ka B.P.) and A.D. 1631 eruptions, there occurred the remaining 22 eruptions; and (3) the area related to VS and AE eruptions that has been possibly lost in the eruptive sequence (possibly older than the Avellino Plinian eruption). SV caldera is outlined in dark orange dashed line.

of uncertainty areas suffers from the limitation that no, or very limited, morphological constraints are available, as the sub-Plinian eruptions resulted in less pronounced caldera collapses/enlargements [*Cioni et al.*, 2008]. For this reason, we have to rely on additional information for the definition of such areas: (a) for the A.D. 1631 eruption, the vent uncertainty area, approximately coinciding with the base of the Gran Cono, is mainly based on historical accounts [*Rosi et al.*, 1993; *Scandone et al.*, 1993; *Nazzaro*, 1997; *Ricciardi*, 2009]; (b) for the A.D. 472 Pollena eruption, due to similarities in magnitude and intensity values, the extent of the vent uncertainty area has been assumed similar to that of A.D 1631 eruption, centered on the Pollena vent location and reshaped according to the SV present caldera outline; (c) for the Greenish Pumice eruption (the oldest among the sub-Plinian I eruptions), uncertainties are greater, as no clear morphological constraint exists due to subsequent activity. For these reasons, the uncertainty area related to this eruption is larger and has been put equal to the one of the closest (in time) Plinian eruption (Pomici di Base).

For sub-Plinian II eruptions (Figure 3c), difficulties are also greater than for the sub-Plinian I eruptions. We adopt, however, a similar approach: (a) for the A.D. 512 eruption, field data [*Cioni et al.*, 2011] and sporadic historical accounts [*Alfano*, 1924] constrain the vent position within the area presently occupied by the Gran Cono, and for this reason, we place the uncertainty area equal to that of the sub-Plinian I A.D. 1631 eruption; (b) for AP1 and AP2 eruptions, *Andronico and Cioni* [2002] provided a reconstruction of fallout isopachs which suggest a vent position in a similar location of the preceding Avellino Plinian eruption. For these reasons, the extent of the uncertainty areas associated to these two eruptions is assumed equal to that adopted for the Avellino eruption.

The large or medium explosive eruption data set is therefore composed of two different feature classes: a point feature class (indicating the centroid of the vent uncertainty area) and a polygon feature class indicating the vent uncertainty areas, both consisting of 10 elements (the 10 eruptions).

In summary, the large- or medium-scale explosive eruption data set highlights how (a) the events do not seem to follow a specific spatiotemporal pattern (i.e., a clear tendency to centralization of volcanic activity is not evident); (b) they are concentrated in three of the four caldera sectors defined in Figure 1, namely, sectors A, B, and D (see also Table 1); and (c) some eruption sites (i.e., the A.D. 79/Mercato/A.D. 512/A.D. 1631, the Greenish Pumices/Pollena, and the Avellino/AP1/AP2 eruptions) appear to be clustered in specific locations close to the NW south-facing rim of the SV caldera, within the Gran Cono edifice and within the "Piano delle Ginestre" area in sector D (Figure 1). However, it should be noted that such spatial variability is restricted within the summit caldera of the SV edifice.

5.3. Vent Location of Small-Scale Explosive Eruptions

The small-scale explosive eruption data set (Figure 4) comprises the violent Strombolian (VS) and continuous ash emission (AE) categories, which have been placed here into one data set to reflect similar magnitudes and intensities, although deposits and related hazards are quite different [*Cioni et al.*, 2008; *Neri et al.*, 2008; *Barsotti et al.*, 2015].

Cioni et al. [2008] report a total of 32 events with field evidences that span a wide temporal window between the Avellino Plinian eruption (4.3 ka B.P.) and the last eruption of 1944. However, the degree of confidence in the vent location for these eruptions is quite variable with respect to time, related to the level of preservation of the associated deposits (which might be easily remobilized and also have a smaller areal extent with respect to higher magnitude/intensity eruptions).

For the younger VS to AE eruptions, i.e., 10 events that occurred after the A.D. 1631 eruption and which have the most preserved deposits, *Arrighi et al.* [2001] were able to reconstruct detailed fallout isopachs, and accordingly, vent positions could be all placed within an area that is approximately coincident with the present rim of Vesuvius crater. For the remaining 22 eruptions that date back to the period between the Avellino and the A.D. 1631 eruption, sparse information has been provided by several authors. Among them, only the AP3 to AP6 eruptions have been systematically studied by *Andronico and Cioni* [2002] and the reconstruction of their fallout isopachs indicates that vent locations for these eruptions were confined to the area of the present edifice of Gran Cono. The remaining eruptions have been cited differently within the bibliographic sources (PM2, PM3, PM4, PM5, and PM6 in *Santacroce and Sbrana* [2003] and AS1a-d, AS2, AS2a-f, AS3, AS4, AS4a-c, and AS5 in *Cioni et al.* [2008]), and the available [*Rolandi et al.*, 1998; *Cioni et al.*, 2008] or unpublished field data indicate that also for these eruptions, the approximate location of the eruptive vent was confined within the area of Gran Cono.

However, the eruptive records of these eruptions might not be complete due to the lower preservation potential with respect to events of higher magnitude or intensity. It is therefore considered the possibility that an unknown number of VS to AE events has been "lost" in the eruptive sequence, and it is proposed to locate these eruptions within an uncertainty area whose extent has been drawn by joining the uncertainty areas of the large- or medium-scale eruptions that occurred before the Avellino eruption (i.e., Pomici di Base, Greenish Pumices, and Mercato). The presence of some scoria cones on the outer SV slopes suggests that midintensity activity sporadically occurred also outside the present SV caldera at different ages (e.g., Pollena and Vallone San Severino scoria cones, between Pomici di Base and Greenish Pumice eruptions; Camaldoli della Torre scoria cone, between the Avellino and the Pompeii eruptions; and several Middle Age scoria cones especially in the southern and western sector of the volcano).

In summary, for the small-scale explosive eruption data set, three main uncertainty areas for the spatial location of vents are defined, each based on the associated time period (Figure 4). These are represented with three feature classes, all of them polygonal. The first comprises a polygonal feature class that accounts for an unknown number of VS to AE eruptions that possibly occurred before the Avellino eruption (Uncertainty_PreAvellino); the second, with extent matching the area of the Gran Cono (Uncertainty_GranCono), is a feature class that represents the uncertainty area of 22 vents from eruptions between the Avellino Plinian eruption and the A.D. 1631 sub-Plinian I eruption; and the third, which is represented by the present crater area, encloses the last 10 VS to AE events, which occurred between the A.D. 1631 and 1944 eruptions (Uncertainty_1944CraterRim).

These three uncertainty areas might suggest that there has been an apparent tendency for volcanic activity to become more centralized through time, in the area of the Gran Cono edifice. Although this might have occurred, the apparent tendency could also reflect the different levels of uncertainty in vent location for the three periods under consideration: older events are simply more uncertain. This said, it is also plausible that they all took place within the same uncertainty areas as the more recent ones. Moreover, the existence of the Gran Cono edifice, which has grown intermittently since the A.D. 79 eruption, might indicate that all known eruptions in this data set contributed to its development.

5.4. Vent Location of Effusive Eruptions

The Effusive eruption data set is composed of two separate subdata sets, i.e., parasitic vent locations and eruptive fissures, which describe the two possible surface manifestations of effusive activity.

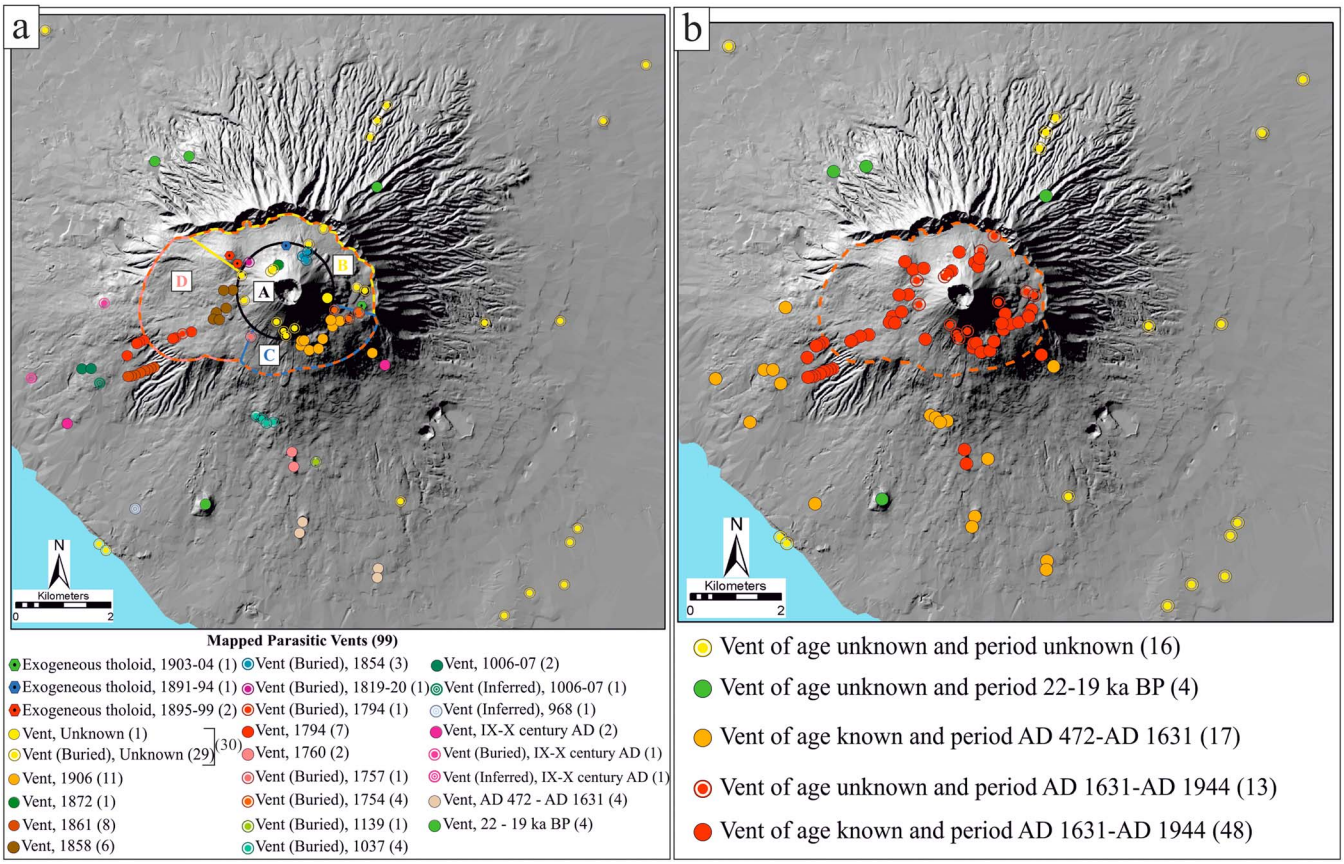

Figure 5. (a) Parasitic vent subdata set. The subdata set was compiled after integration of several bibliographic sources (see section 5.4.1). SV caldera is outlined in dark orange dashed line; the four sectors partitioning the caldera have the colors reported in the legend; (b) parasitic vents grouped by different time periods.

5.4.1. Parasitic Vents

The term "parasitic vents" refers here to any punctual (i.e., not fissural) surface expression of lava or scoria emission along the flanks of the main edifice; scoria cones, vents aligned along eruptive fissures (described in section 5.4.2), isolated vents ("bocche"), and exogenous tholoids (local accumulation of lava that creates significant reliefs) are included in this data set, whereas rootless vents ("hornitos") are not considered.

A total of 95 vents (47 with surface exposure, 45 buried, and 3 inferred) and 4 exogenous tholoids totaling 99 parasitic vents have been mapped over the whole SV complex (Figure 5a), after integration of several

Table 2. Summary Table of Parasitic Vents as Discussed in the Text[a]

	MAPPED			Bibliography (min–max)	Lost Vents (min–max)
Sector	Age Known	Age Unknown	Total	Total	Total
A	6	9	15	29–42	14–27
B	3	4	7	11–13	4–6
C	14	–	14	14	–
D	10	–	10	10	–
Unknown	–	–	–	19–23	19–23
Inside caldera	33	13 (<A.D. 1631)	46	83–102	37–56
Outside caldera (age < A.D. 1631)	15	–	15	15–21	0–6
TOT (age < A.D. 1631)	48	13	61	98–123	37–62
Outside caldera (all ages)	27	26	53	–	–
TOT (all ages)	69	30	99	–	–

[a]Sectors as defined in Figures 1 and 5 and section 5.1. The notations min and max refer, respectively, to the minimum and maximum numbers of vents cited in the bibliographic sources considered and of "lost vents" (difference between vents cited in bibliography and mapped vents, see section 5.4.1 and Appendix A for more details).

bibliographic sources [*Bertagnini et al.*, 1991; *Bruno and Rapolla*, 1999; *Cioni et al.*, 2008; *IGM*, 1876, 1906; *Principe et al.*, 2013; *Santacroce*, 1987; *Santacroce and Sbrana*, 2003; *Ventura et al.*, 2005].

With respect to spatial location (Table 2), 46 out of 99 vents/tholoids are located within the SV caldera and, among them, 15 are located within sector A, 7 within sector B, 14 within sector C, and 10 within sector D (Figure 5a). Parasitic vents located outside the SV caldera (53 vents) are generally concentrated in the south, where most of them have surface exposure, while several of them have been identified from seismic surveys [*Bruno and Rapolla*, 1999; *Ventura et al.*, 2005] or have been inferred from considerations on lava flow morphologies [*Principe et al.*, 2013].

As far as times of vent formation are concerned (Table 2), 48 vents out of 99 are related to eruptions which occurred after the A.D. 1631 eruption, 21 to eruptions that occurred between the Pomici di Base and the A.D. 1631 eruptions, while 30 vents are classified as "age unknown," and they were not assigned to any of the known eruptions of SV (Table 2 and Figure 5a). Several assumptions about their ages can be made: (i) it is reasonable to assume that vents within the SV caldera (13 vents) are likely to be representative of the period 1631–1944 (Plinian caldera-forming eruptions and sub-Plinian eruptions likely obliterated vents that preceded them); (ii) for the rest (16 vents), the possibility that they took place within the period 1631–1944 can be excluded because all the vents within this period outside SV caldera have been mapped from reliable historical chronicles; (iii) vents outside SV caldera and located to the north/northeast/northwest of Mount Somma scarp (six vents) are probably related to Mount Somma activity or to Vesuvius activity up to the Pompeii eruption—there is an absence of records of eccentric activity in historical chronicles for this sector, and the three parasitic vents on Mount Somma scarp date to before the Pomici di Base eruption; and (iv) for vents outside SV caldera and located to the east/west/southeast/southwest (10 vents), it is too speculative to attribute ages since, in this part of the volcano, eruptive centers opened even after the Pompeii eruption, although some of them might be related to effusive volcanic activity that occurred between the IX and X centuries C.E. [*Principe et al.*, 2004]. Very recently, some buried effusive volcanic vents have been possibly identified by *Paoletti et al.* [2016], off the coast of Torre del Greco.

To better highlight the distribution of parasitic vents with respect to different time periods, a summary has been compiled in Figure 5b. This figure shows how the parasitic vents, at least within the last 400 years, are uniformly spread over the whole caldera area, with some located outside as well. In contrast, the still-visible vents related to the period A.D. 472 to A.D. 1631 are all located outside the SV caldera; however, it is impossible to assess whether or not others opened inside the caldera during the same period, since subsequent eruptions will likely have obliterated any sign of them.

When assessing uncertainties related to location of parasitic vents, two different sources of uncertainty need to be considered. The first is related to spatial uncertainties in feature location, related to possible errors due to inaccurate placement of vents from field data to maps, for which appropriate uncertainty areas have been defined; the second arises from the comparison between the positions of vents mapped in the field and the locus of vents cited in historical accounts (from which we derive an estimate of the number of "lost vents"). Due to several residual ambiguities and discrepancies among the different historical accounts considered (for instance, a different source might cite different numbers of parasitic vents for the same eruption), the number of lost vents could be estimated only as a range (minimum and maximum values). In this case it has been considered not necessary to define uncertainty areas with different dimensions for each parasitic vent since the differences among them have been considered minimal.

In the case of parasitic vents, their locations have been determined mostly from existing databases and maps with precise geographic coordinates and reference points, resulting in apparent very low positioning errors. However, several mapped vents have presently limited exposure or are completely buried, whereas others have been deduced from seismic reflection surveys [*Bruno and Rapolla*, 1999]. Based on these limitations and considering the typical measured radius of scoria cone craters in different volcanic settings [*Corazzato and Tibaldi*, 2006; *Dóniz et al.*, 2008; *Hasenaka and Carmichael*, 1985; *Porter*, 1972], a circular uncertainty area with radius 75 m is assumed for all parasitic vents.

With the goal of estimating the second element of uncertainty, i.e., the number of lost vents, a detailed analysis and comparison of bibliographic sources dealing with parasitic vent locations has been carried out by analyzing bibliographic sources that summarize the observations recorded in historical accounts

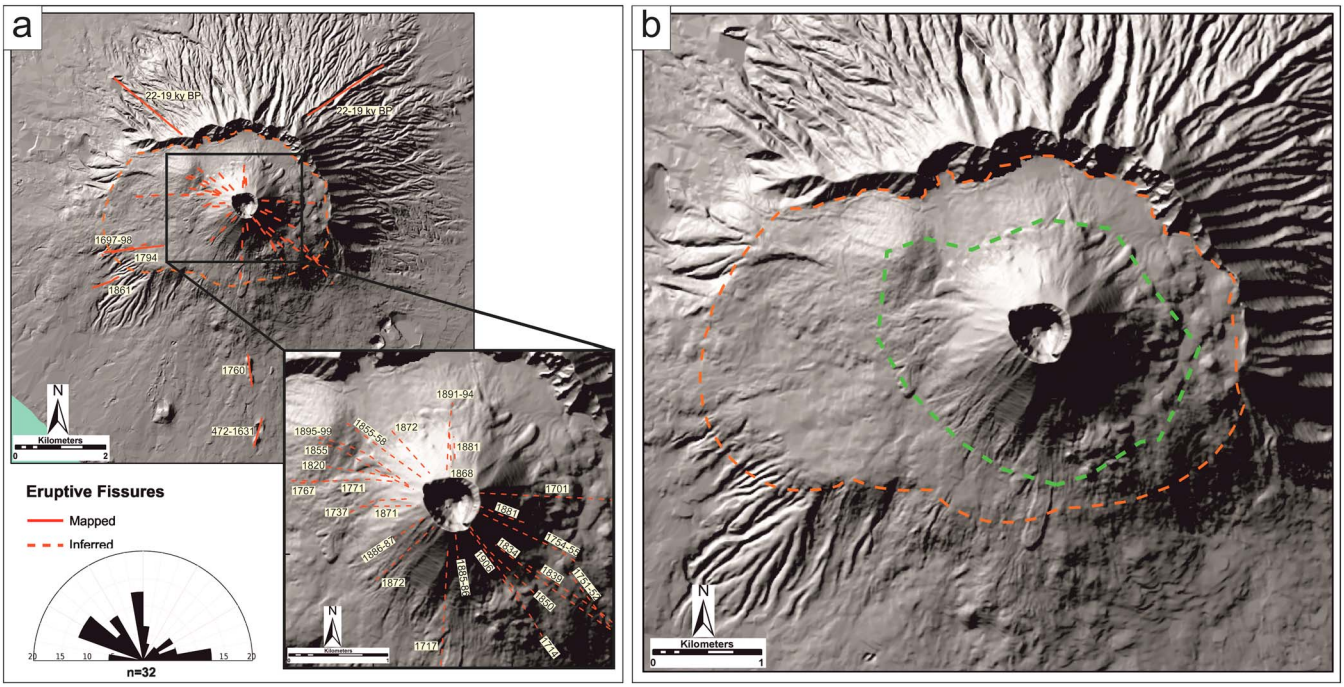

Figure 6. Eruptive fissures subdata set. (a) Eruptive fissure subdata set compiled after integration of different bibliographic sources (see section 5.4.2). The numbers in yellow boxes are ages of eruptive fissures. The rose diagram refers to all eruptive fissures in the data set (petal size is 10°); (b) high-density area for eruptive fissures (in light green dashed line) as discussed in section 5.4.2. SV caldera outlined in dark orange dashed line.

[*Nazzaro*, 1997; *Ricciardi*, 2009; *Scandone et al.*, 1993]. Chronicles and historical accounts about this topic are very poor before the year 1631, and therefore, the comparison performed in this work was restricted to the period 1631–1944. A detailed comparative table is reported in Table S1 in the supporting information, and more details about the procedure are provided in Appendix A. Table 2 reports the minimum and maximum (min; max) numbers of parasitic vents as deduced from such bibliographic sources and historical accounts and hence indicates the potential numbers of lost vents. With the information available it is also possible to define qualitatively the position of several vents cited in the bibliography by using SV caldera morphological sectors (Figure 1b). It is estimated that 37–62 vents should be considered "lost vents"; apart from these latter ones, it is worth noting that five vents have been mapped but are not cited in the historical records (1757, 1854, and 1872 eruptions). Among these, it is estimated that between 14 and 27 lost vents could have been located in sector A, 4–6 in sector B, 19–23 within the whole caldera, and 0–5 outside the SV caldera.

5.4.2. Eruptive Fissures

The term "eruptive fissure" refers here to any fracture on the volcanic edifice from which emission of volcanic materials (lava, ash, and scoriae) has taken place. Eruptive fissures at SV generally resulted in the emission of lava through gentle effusions and/or fountaining (e.g., 1779 and 1872 eruptions [*Scandone et al.*, 1993]). At least in one case, during the A.D. 1631 eruption [*Rosi et al.*, 1993], the initial fracture rapidly evolved into a point vent and was clearly characterized by emission of ash, scoriae, and incandescent blocks, without any lava effusions.

This subdata set is composed of 32 elements (Figure 6a), derived from several papers and geological maps [*Santacroce*, 1987; *Santacroce and Sbrana*, 2003; *Acocella et al.*, 2006a; *Cioni et al.*, 2008]. Among them, only 6 cases out of 32 can still be mapped in the field, while the locations of the rest are simply inferred from bibliographic sources [*Acocella et al.*, 2006a]. A total of 27 fissures developed wholly, or almost entirely, within the SV caldera. Ages of different eruptive fissures, as defined in *Acocella et al.* [2006a], have been confirmed by comparison with other bibliographic sources and dated geological units underlying or in proximity to the assumed eruptive fissure [*Santacroce and Sbrana*, 2003]. A total of seven fissures drawn by *Acocella et al.* [2006a], whose positions are not attributable with a sufficient degree of confidence, have not been included in the present data set. These fissures were related to the eruptions of 1631 (although *Rosi et al.* [1993]

showed a preferred site of the fissure location within the W flank of the previous edifice), 1694, 1723, 1766, 1804–1805, and 1822 (the latter associated to two fissures, as reported by *Acocella et al.* [2006b]). From the point of view of ages, the bulk of eruptive fissures (29 of 32) were related to the period 1631–1944. A comparison is made of different bibliographic sources which analyze historical accounts between the A.D. 1631 and the 1944 eruptions [*Acocella et al.*, 2006a; *Ricciardi*, 2009; *Scandone et al.*, 1993], similar to that performed for parasitic vents, in order to account for possible "lost eruptive fissures" and to provide robust estimates for the locations of those eruptive fissures already included in the data set. The result of this detailed comparison and of the comparison between parasitic vents and eruptive fissures for a single eruption is available in Table S2 and in Appendix B. Considering the three sources cited in the previous paragraph as a whole, eruptive fissures have been reported from 52 eruptions within the period 1631–1944, resulting in the formation of 57–67 eruptive fissures (numbers have the same meaning of those used for parasitic vents, i.e., min–max range), and the number of "lost" features is 28–38.

Location uncertainties for eruptive fissures are evaluated in a similar way as for parasitic vents. Eruptive fissures are digitized in vector format by georeferencing a raster image from *Acocella et al.* [2006b]. However, as discussed before, these locations potentially are affected by substantial uncertainty as the positions of most (i.e., 26 of 32) have been inferred from descriptions in the chronicles and not directly mapped in the field. This situation is particularly evident for the fissures located in the area of Gran Cono (Figure 6a), today completely covered under a thick pile of recent lava flows. In consequence, a possible approach for using this fissure data set (limited to the area of Gran Cono) is to define a high-density area of eruptive fissures. Such an area (see Figure 6b) roughly includes the entire Gran Cono up to its base and is slightly elongated along the NW-SE direction following one of the prevailing trends of eruptive fissures (see rose diagram inset in Figure 6a). As further discussed in *Tadini et al.* [2017], a circular uniform distribution of eruptive fissures can be assumed within such an area, as fissures around the Gran Cono are mainly radially distributed (Figure 6a).

Locations for a number of "lost eruptive fissures" can be qualitatively given with a certain degree of confidence by considering the disposition of past eruptive fissures with respect to the volcanic edifice. *Acocella et al.* [2006a, 2006b] have extensively treated this topic, showing an almost radial disposition of fissures with respect to the Vesuvius cone for the 1631–1944 eruptive period. Figure 6a clearly illustrates this general radial trend, although it also shows some prevalence of fissures mainly along the NW-SE direction (and partially along E-W direction), consistent with the orientation of the regional stress field and NW-SE trending regional structures (Figure 1a; see also section 5.5). "Lost eruptive fissures" should thus be located in an area roughly corresponding to the above-mentioned uncertainty high-density area of eruptive fissures.

5.5. Deep Faults (Buried)

The deep fault data set (Figure 7) is composed of a linear feature class with 54 elements representing faults detected in the substratum. These faults derive from previous studies and were identified and characterized through seismic reflection methods (45 faults, 35 after interpolation and 10 after extrapolation [*Bianco et al.*, 1998; *Bruno et al.*, 1998; *Bruno and Rapolla*, 1999]), gravimetric data (six faults [*Cassano and La Torre*, 1987]), or mixed gravimetric and seismic reflection data (three faults classified as "neotectonic structures" by *Ciaranfi et al.* [1981]). Seven out of 54 faults cross the SV caldera, as defined in the present work, two of them being located with mixed gravimetric/seismic data and the remaining five with geophysical data. Notably, the two faults that cross SV caldera, as evidenced by *Ciaranfi et al.* [1981], mimic the position and strike of other faults extrapolated from seismic profiles by *Bruno et al.* [1998], suggesting that they likely represent the same fault planes.

Lengths of deep faults vary between about 400 m and 13.5 km and show a rather tight distribution along the NE-SW and NW-SE directions (Figure 7 [*Bianco et al.* [1998]). All these faults cut through the Mesozoic carbonate basement [*Ciaranfi et al.*, 1981; *Cassano and La Torre*, 1987; *Bianco et al.*, 1998; *Bruno et al.*, 1998] or within the shallower 150–200 m of alluvial/volcanic deposits [*Bruno and Rapolla*, 1999]. The top of the carbonate basement underneath the Campanian plain has been calculated from geophysical data inversion [*Bruno et al.*, 1998] and gravimetric data [*Cella et al.*, 2007] and varies from more than 2000 m below sea level (bsl) in the Acerra and Pompeii grabens, up to shallower depths (1400–1500 m bsl) below the SV area., where it was drilled by the Trecase geothermal well. Extrapolation of fault planes from geophysical

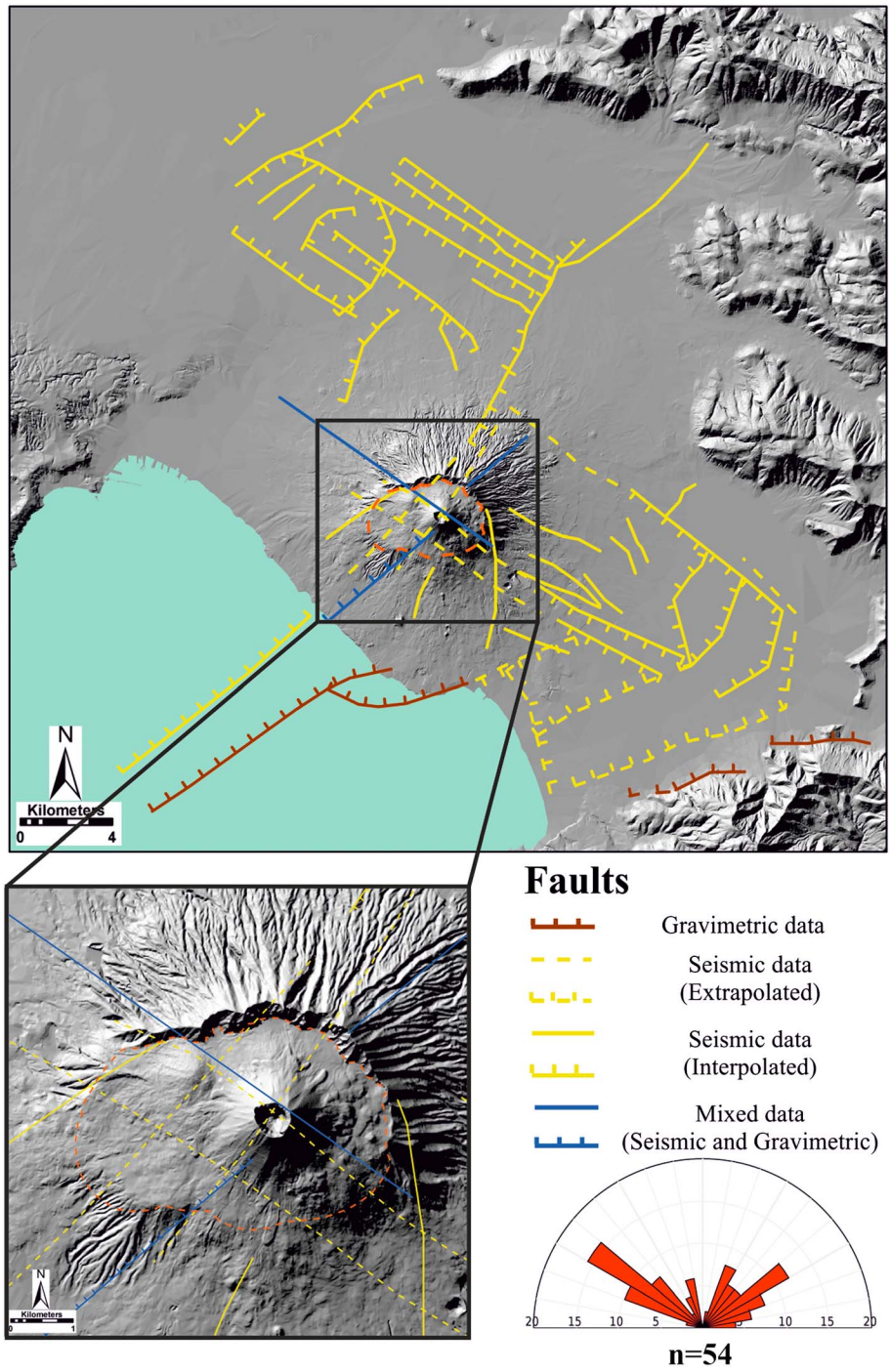

Figure 7. Deep fault data set. Deep fault data set compiled after integration of different bibliographic sources (see section 5.5). The petal size of related rose diagrams is 10°.

profiles has been put forward by *Bruno et al.* [1998] as well, with specific focus on structures that cut the SV caldera (Figure 7). These inferred faults are consistent with numerous observations of fault planes from other sources [*Cassano and La Torre*, 1987; *Ciaranfi et al.*, 1981; *Florio et al.*, 1999]. *Bianco et al.* [1998] point out that local fault kinematics at SV are also consistent with regional fault kinematics that is normal to sinistral for the NW-SE trending faults and normal to dextral for the NE-SW trending structures (see section 2.1).

For the deep fault data set, a linear uncertainty area is assumed here with a width of 150 m, a value that accounts for the resolution limits of the seismic profiles employed for the recognition of the faults of this data set.

The deep fault data set suggests that—for the SV caldera area—the intersection of two faults in the E part of the caldera coincides with the position of the Gran Cono edifice. Moreover, the intersection of these faults, and of other two faults close to the NW south-facing rim of the caldera, might be correlated with the position of some large- or medium-scale explosive eruption sites (see section 5.2). Although it is often accepted that a stratovolcano forms at the intersection of major fault planes [e.g., *Kyle and Cole*, 1974], proposing that this is the case for the SV volcano is, currently, speculative; the extents of some of the faults in this data set have been extrapolated, and hence, their reliability is questionable.

6. Concluding Remarks

New and revised data sets of the eruptive and structural features of the Somma-Vesuvio volcanic complex have been developed with the aim of synthesizing a uniform geodatabase that complements and extends existing data sets. These data sets relate specifically to a new reconstruction of the inferred locations of past eruptive vents and fissures of SV activity and to some regional/local structures, with emphasis being placed on enumerating associated uncertainties. Such information is relevant for assessing present limitations on our knowledge of SV eruptive history and for producing more accurate hazard assessment studies. SV clearly shows a significant spatial variability in its past activity as a function of time and type of eruption. Field evidence and theoretical studies show that such variability can significantly affect the areas impacted by erupted products and attention to localities that might potentially be inundated by pyroclastic density currents is warranted.

The important specific attribute of the new data sets is the consideration and quantification of spatial uncertainty and the extent to which it influences the reconstruction and interpretation of such information. Here the evaluation and use of uncertainty areas and of boundaries to topological features, delineated to encompass fully their positional imprecision, provide a coherent basis for enumerating the related uncertainties. For the parasitic vents and eruptive fissure subdata sets, the number of features that have been recorded in historical accounts but have been obliterated by subsequent eruptions (i.e., "lost vents" and "lost fissures") has been calculated as well. This innovative feature of the data sets serves to reflect quantitatively the intrinsic uncertainty that attends such information.

All the new data about uncertainty areas and the revised data sets are assembled in a volcanological geodatabase, complementing existing individual topic and separate subject matter SV databases. This unifying geodatabase can be queried and updated and is currently under further development with the inclusion of further new or revised data and information about past activity (i.e., isopachs of PDCs and fallout thickness, lahar inundation areas, and geochemical and geophysical data). Because the new database includes specific information on some sources of uncertainty affecting the data, it also represents a valuable source of information for the development of hazard assessment products.

In *Tadini et al.* [2017] the data sets presented here are used to produce a first quantitative background (or long-term) vent opening probability map of the SV caldera, with specific reference to the occurrence of sub-Plinian and Plinian events. This approach is, therefore, consistent with good practice in other volcanic areas where better information and more plentiful data are available [*Cappello et al.*, 2012; *Connor et al.*, 2012; *Bartolini et al.*, 2013; *Bevilacqua et al.*, 2015].

Finally, qualitative inspection of the data sets here considered allows to draw some consideration with respect to the spatiotemporal distribution of volcanic activity source at SV: (a) the initial vent of all Plinian and sub-Plinian eruptions was located within, or near, the outer rim of the SV caldera, as it existed at the time (moreover, several of the eruption sites seem to be concentrated in three main locations, i.e., the Gran Cono area, the "Piano delle Ginestre" area, and an area close to the NW rim of the caldera); (b) there is an apparent tendency for the centralization, during the most recent history of the volcano, of eruptive activity in the area of the Gran Cono edifice, but this is only particularly evident by looking at the violent Strombolian to continuous ash emission eruption data set, which might be incomplete. This possibility needs to be evaluated with more dedicated studies, which should address whether this tendency is due to the effect of edifice loading

focusing rising dikes [*Muller et al.*, 2001], or to other factors; (c) the parasitic vent eruption data set does not evince a particular temporal trend with respect to spatial distribution (following *Acocella et al.* [2006a], parasitic effusive activity at SV, i.e., vents and fissures, might be associated with open conduit conditions and horizontally developed radial dikes); (d) the Gran Cono edifice and two groups of Plinian and sub-Plinian eruptions are located at the intersection of two pairs of extrapolated or inferred fault planes; the limited reliability of information on such faults within the deep faults data set means that any other interpretation is highly speculative.

Appendix A: Analysis of the Positional Uncertainty for Parasitic Vents

This appendix provides more details to the analysis about the discrepancies (among different bibliographic sources) of the number of parasitic vents that occurred during different SV eruptions, which are here coded through the notation "*x*/*y*": these two numbers indicate, respectively, the sum of all vents calculated using (for eruption with discrepancies) the minimum (*x*) and maximum (*y*) number of cited vents. For example, considering the 1794 eruption, we have four vents from *Scandone et al.* [1993], eight vents from *Nazzaro* [1997], and six vents from *Ricciardi* [2009]. In this case the minimum and maximum are 4 and 8, respectively. Table 1 reports such values in the "Bibliography MIN/MAX" column. Considering the three sources as a whole, parasitic vents have been reported for 27 different eruptions between 1723 and 1906 eruptions with a total number of vents from 98 to 123 (Table 2). With the information available we were able to define qualitatively the positions of the vents cited in bibliography using SV caldera morphological sectors (Figure 1b): as an example, parasitic vents from the May 1858 to April 1861 eruption cited by *Scandone et al.* [1993] were placed in sector D of SV caldera because the authors provided as location site for these vents the "Piano delle Ginestre" area (see Table S1 for more details). Within SV caldera sectors (Figure 5a), we were able to assign 29–42 vents to sector A, 11–13 vents to sector B, 14 vents to sector C, 10 vents to sector D, 19–23 vents with an unknown localization within the whole caldera, and 15–20 vents outside the SV caldera.

Table S1 provides a comparison between numbers of parasitic vents as reconstructed by three different bibliographic sources and for eruptions that occurred after the A.D. 1631 sub-Plinian I eruption. For each record, the number of vents reported in each source is provided and, where possible, qualitative indications about vent locations. The black records represent eruptions with parasitic vents cited only in one source; the light blue records represent eruptions with parasitic vents cited in two sources or cited in all the three sources but with differences in vent number; the red records indicate eruptions with full agreement among the sources. Data from *Nazzaro* [1997] and *Ricciardi* [2009] are underestimated due to ambiguities in vent citations for some eruptions.

Appendix B: Analysis of the Positional Uncertainty for Eruptive Fissures

Similar to parasitic vents, eruptive fissures also show discrepancies among different bibliographic sources (Table S2) and between these and the fissures mapped, resulting in a certain number of "lost eruptive fissures." With respect to the 29 fissures mapped or inferred (over the period between A.D. 1631 and 1944), the number of "lost eruptive fissures" is 28–38 (here the notation is the same as that used for parasitic vents).

Table S2 provides a comparison between three different bibliographic sources for eruptions that occurred after the A.D. 1631 sub-Plinian I eruption. For each record, the number of fissures reported in each source is provided and, where possible, qualitative indications about fissure locations. The black records represent eruptions with fissures cited only in one source; the light blue records represent eruptions with fissures cited in two sources or cited in all the three sources but with differences in the number of fissures; the red records indicate eruptions with full agreement among the sources.

Eruptive fissures could be closely related to parasitic vents because, for several fissures, their linear development is marked by an alignment of parasitic vents (e.g., 1760, 1794, and 1861 eruptions; Figure 5a [*Scandone et al.*, 1993]). Table S3 provides a comparison between different eruptions (from the period 1631 to 1944) and the occurrence of vents versus eruptive fissures for each eruption. From this table it is possible to evaluate that for 17 eruptions, bibliographic sources report the contemporaneous occurrence of eruptive fissures and parasitic vents. Among these events it was possible to estimate that for seven of them (1754–1755,

1760–1761, 1794, 1861, 1891–1894, 1895–1999, and 1906) 24 mapped parasitic vents were located along their related eruptive fissures, while for the remaining 10 (1723, 1737, 1751, 1819–1820, 1821, 1822, 1834, 1855, 1855–1858, and 1903–1904) this relation is either absent or not demonstrable. Four other parasitic vents from earlier ages are located along eruptive fissures as well.

Authors' Contributions

A.T. and R.C. participated in the definition of the new data sets, retrieval of data from bibliography, and organization of the different data sets. A.T. and M.B. developed the geodatabase and implemented the different data sets. A.T., A.B., A.N., R.C., and W.A. contributed to the construction and implementation of the uncertainty areas and discussed of their probabilistic interpretation. A.T. and A.N. mostly contributed to the writing of the manuscripts, but all authors contributed to its revision and improvements.

Acknowledgments

This work has been partially supported by the project V1 "Stima della pericolosità vulcanica in termini probabilistici" funded by the Dipartimento della Protezione Civile (Italy) and by the project MEDSUV "Mediterranean Supersite Volcanoes" funded by the European Union (grant 308665). W.P.A. was supported in part at Bristol University by the CREDIBLE Consortium funded by the UK Natural Environment Research Council (grant NE/J017299/1). Marco Bocci from Istituto Geografico Militare (IGM) is greatly acknowledged for kindly allowing the consultation of the IGM archive for retrieval of historical maps for the Somma-Vesuvio area. Mike Poland, Heather Wright, and an anonymous reviewer are gratefully thanked for their insightful comments and constructive suggestions that greatly improved the quality of the manuscript. The new and revised data sets presented in this study as well as the access to the geodatabase developed are available from the Data Set S1 file in the supporting information.

References

Acocella, V., M. Porreca, M. Neri, M. Mattei, and R. Funiciello (2006a), Fissure eruptions at Mount Vesuvius (Italy): Insights on the shallow propagation of dikes at volcanoes, *Geology*, *34*(8), 673–676.

Acocella, V., M. Porreca, M. Neri, E. Massimi, and M. Mattei (2006b), Propagation of dikes at Vesuvio (Italy) and the effect of Mt. Somma, *Geophys. Res. Lett.*, *33*, L08301, doi:10.1029/2005GL025590.

Aiuppa, A., A. Caleca, C. Federico, S. Gurrieri, and M. Valenza (2004), Diffuse degassing of carbon dioxide at Somma-Vesuvius volcanic complex (southern Italy) and its relation with regional tectonics, *J. Volcanol. Geotherm. Res.*, *133*(1), 55–79.

Alfano, G. B. (1924), Le Eruzioni del Vesuvio tra il 79 e il 1631: Studio bibliografico, Scuola Tipografica Pontifica per i Figli dei Carcerati.

Andronico, D., and R. Cioni (2002), Contrasting styles of Mount Vesuvius activity in the period between the Avellino and Pompeii Plinian eruptions and some implications for assessment of future hazards, *Bull. Volcanol.*, *64*(6), 372–391.

Arrighi, S., C. Principe, and M. Rosi (2001), Violent strombolian and subplinian eruptions at Vesuvius during post-1631 activity, *Bull. Volcanol.*, *63*(2–3), 126–150.

Aspinall, W. P. (2006), Structured elicitation of expert judgment for probabilistic hazard and risk assessment in volcanic eruptions, *Stat. Volcanol.*, *1*, 15–30.

Auger, E., P. Gasparini, J. Virieux, and A. Zollo (2001), Seismic evidence of an extended magmatic sill under Mt. Vesuvius, *Science*, *294*(5546), 1510–1512.

Barsotti, S., A. Neri, A. Bertagnini, R. Cioni, M. Mulas, and F. Mundula (2015), Dynamics and tephra dispersal of violent Strombolian eruptions at Vesuvius: Insights from field data, wind reconstruction and numerical simulation of the 1906 event, *Bull. Volcanol.*, *77*(7), 1–19.

Bartolini, S., A. Cappello, J. Martí Molist, and C. Del Negro (2013), QVAST: A new quantum GIS plugin for estimating volcanic susceptibility, *Nat. Hazards Earth Syst. Sci.*, *13*, 3031–3042.

Berrino, G., G. Corrado, and U. Riccardi (1998), Sea gravity data in the Gulf of Naples: A contribution to delineating the structural pattern of the Vesuvian area, *J. Volcanol. Geotherm. Res.*, *82*(1), 139–150.

Bertagnini, A., P. Landi, R. Santacroce, and A. Sbrana (1991), The 1906 eruption of Vesuvius: From magmatic to phreatomagmatic activity through the flashing of a shallow depth hydrothermal system, *Bull. Volcanol.*, *53*(7), 517–532.

Bertagnini, A., P. Landi, M. Rosi, and A. Vigliargio (1998), The Pomici di Base Plinian eruption of Somma-Vesuvius, *J. Volcanol. Geotherm. Res.*, *83*(3), 219–239.

Bevilacqua, A. (2016), Doubly stochastic models for volcanic hazard assessment at Campi Flegrei caldera, PhD thesis, 184 pp., Edizioni della Normale, Birkhäuser/Springer.

Bevilacqua, A., et al. (2015), Quantifying volcanic hazard at Campi Flegrei caldera (Italy) with uncertainty assessment: I. Vent opening maps, *J. Geophys. Res. Solid Earth*, *120*, 2309–2329, doi:10.1002/2014JB011775.

Bevilacqua, A., F. Flandoli, A. Neri, R. Isaia, and S. Vitale (2016), Temporal models for the episodic volcanism of Campi Flegrei caldera (Italy) with uncertainty quantification, *J. Geophys. Res. Solid Earth*, *121*, 2169–9356, doi:10.1002/2016JB013171.

Bianco, F., M. Castellano, G. Milano, G. Ventura, and G. Vilardo (1998), The Somma-Vesuvius stress field induced by regional tectonics: Evidences from seismological and mesostructural data, *J. Volcanol. Geotherm. Res.*, *82*(1), 199–218.

Bruno, P. P. G., and A. Rapolla (1999), Study of the sub-surface structure of Somma-Vesuvius (Italy) by seismic reflection data, *J. Volcanol. Geotherm. Res.*, *92*(3), 373–387.

Bruno, P. P. G., G. Cippitelli, and A. Rapolla (1998), Seismic study of the Mesozoic carbonate basement around Mt. Somma-Vesuvius, Italy, *J. Volcanol. Geotherm. Res.*, *84*(3), 311–322.

Cappello, A., M. Neri, V. Acocella, G. Gallo, A. Vicari, and C. Del Negro (2012), Spatial vent opening probability map of Etna volcano (Sicily, Italy), *Bull. Volcanol.*, *74*(9), 2083–2094.

Cassano, E., and P. La Torre (1987), *Geophysics, Somma-Vesuvius*, *Quad. Ric. Sci.*, vol. 8, pp. 175–195, CNR, Roma, Italy.

Cella, F., M. Fedi, G. Florio, M. Grimaldi, and A. Rapolla (2007), Shallow structure of the Somma-Vesuvius volcano from 3D inversion of gravity data, *J. Volcanol. Geotherm. Res.*, *161*(4), 303–317.

Ciaranfi, N., A. Cinque, S. Lambiase, P. Pieri, L. Rapisardi, G. Ricchetti, I. Sgrosso, and L. Tortorici (1981), Proposta di zonazione sismotettonica dell'Italia Meridionale, *Rend. Soc. Geol. Ital.*, *4*, 493–496.

Cioni, R., R. Santacroce, and A. Sbrana (1999), Pyroclastic deposits as a guide for reconstructing the multi-stage evolution of the Somma-Vesuvius caldera, *Bull. Volcanol.*, *61*(4), 207–222.

Cioni, R., S. Levi, and R. Sulpizio (2000), Apulian Bronze Age pottery as a long-distance indicator of the Avellino Pumice eruption (Vesuvius, Italy), *Geol. Soc. London, Spec. Publ.*, *171*(1), 159–177.

Cioni, R., R. Sulpizio, and N. Garruccio (2003), Variability of the eruption dynamics during a subplinian event: The Greenish Pumice eruption of Somma-Vesuvius (Italy), *J. Volcanol. Geotherm. Res.*, *124*(1), 89–114.

Cioni, R., A. Bertagnini, R. Santacroce, and D. Andronico (2008), Explosive activity and eruption scenarios at Somma-Vesuvius (Italy): Towards a new classification scheme, *J. Volcanol. Geotherm. Res.*, *178*(3), 331–346.

Cioni, R., A. Bertagnini, D. Andronico, P. D. Cole, and F. Mundula (2011), The 512 A.D. eruption of Vesuvius: Complex dynamics of a small scale subplinian event, *Bull. Volcanol.*, *73*(7), 789–810.
Connor, L. J., C. B. Connor, K. Meliksetian, and I. Savov (2012), Probabilistic approach to modeling lava flow inundation: A lava flow hazard assessment for a nuclear facility in Armenia, *J. Appl. Volcanol.*, *1*(1), 1–19.
Cooke, R. M. (1991), *Experts in Uncertainty: Opinion and Subjective Probability in Science*, 320 pp., Oxford Univ. Press.
Corazzato, C., and A. Tibaldi (2006), Fracture control on type, morphology and distribution of parasitic volcanic cones: An example from Mt. Etna, Italy, *J. Volcanol. Geotherm. Res.*, *158*(1–2), 177–194.
De Natale, G., C. Troise, F. Pingue, G. Mastrolorenzo, and L. Pappalardo (2006), The Somma-Vesuvius volcano (southern Italy): Structure, dynamics and hazard evaluation, *Earth Sci. Rev.*, *74*(1–2), 73–111.
De Siena, L., E. Del Pezzo, F. Bianco, and A. Tramelli (2009), Multiple resolution seismic attenuation imaging at Mt. Vesuvius, *Phys. Earth Planet. Inter.*, *173*(1), 17–32.
Del Pezzo, E., F. Bianco, L. De Siena, and A. Zollo (2006), Small scale shallow attenuation structure at Mt. Vesuvius, Italy, *Phys. Earth Planet. Inter.*, *157*(3), 257–268.
Di Renzo, V., M. A. Di Vito, I. Arienzo, A. Carandente, L. Civetta, M. D'antonio, F. Giordano, G. Orsi, and S. Tonarini (2007), Magmatic history of Somma-Vesuvius on the basis of new geochemical and isotopic data from a deep borehole (Camaldoli della Torre), *J. Petrol.*, *48*(4), 753–784.
Dóniz, J., C. Romero, E. Coello, C. Guillén, N. Sánchez, L. García-Cacho, and A. García (2008), Morphological and statistical characterisation of recent mafic volcanism on Tenerife (Canary Islands, Spain), *J. Volcanol. Geotherm. Res.*, *173*(3–4), 185–195.
Engwell, S. L., W. P. Aspinall, and R. S. J. Sparks (2015), An objective method for the production of isopach maps and implications for the estimation of tephra deposit volumes and their uncertainties, *Bull. Volcanol.*, *77*(7), 1–18.
Esposti Ongaro, T., A. Neri, G. Menconi, M. De'Michieli Vitturi, P. Marianelli, C. Cavazzoni, G. Erbacci, and P. J. Baxter (2008a), Transient 3D numerical simulations of column collapse and pyroclastic density current scenarios at Vesuvius, *J. Volcanol. Geotherm. Res.*, *178*(3), 378–396.
Esposti Ongaro, T., P. Marianelli, M. Todesco, A. Neri, C. Cavazzoni, and G. Erbacci (2008b), Mappe tematiche, geo-referenziate e digitali, delle principali azioni pericolose associate alle colate piroclastiche del Vesuvio e dei Campi Flegrei derivanti dalle nuove simulazioni 3D, Prodotto 2.3.5, Progetto SPEED.
Federico, C., A. Aiuppa, R. Favara, S. Gurrieri, and M. Valenza (2004), Geochemical monitoring of groundwaters (1998–2001) at Vesuvius volcano (Italy), *J. Volcanol. Geotherm. Res.*, *133*(1–4), 81–104.
Ferrucci, F., G. Gaudiosi, N. A. Pino, G. Luongo, A. Hirn, and L. Mirabile (1989), Seismic detection of a major Moho upheaval beneath the Campania volcanic area (Naples, southern Italy), *Geophys. Res. Lett.*, *16*(11), 1317–1320, doi:10.1029/GL016i011p01317.
Finetti, I., and C. Morelli (1974), Esplorazione sismica a riflessione dei Golfi di Napoli e Pozzuoli, *Boll. Geofis. Teor. Appl.*, *16*(62/63), 175–222.
Florio, G., M. Fedi, F. Cella, and A. Rapolla (1999), The Campanian Plain and Phlegrean Fields: Structural setting from potential field data, *J. Volcanol. Geotherm. Res.*, *91*(2), 361–379.
Frondini, F., G. Chiodini, S. Caliro, C. Cardellini, D. Granieri, and G. Ventura (2004), Diffuse CO_2 degassing at Vesuvio, Italy, *Bull. Volcanol.*, *66*(7), 642–651.
Granieri, D., M. L. Carapezza, R. Avino, C. Cardellini, M. Donnini, M. Ranaldi, and L. Tarchini (2013), Level of carbon dioxide diffuse degassing from the ground of Vesuvio: Comparison between extensive surveys and inferences on the gas source, *Ann. Geophys.*, *56*, 4.
Gurioli, L., B. F. Houghton, K. V. Cashman, and R. Cioni (2005), Complex changes in eruption dynamics during the 79 A.D. eruption of Vesuvius, *Bull. Volcanol.*, *67*(2), 144–159.
Gurioli, L., R. Sulpizio, R. Cioni, A. Sbrana, R. Santacroce, W. Luperini, and D. Andronico (2010), Pyroclastic flow hazard assessment at Somma-Vesuvius based on the geological record, *Bull. Volcanol.*, *72*(9), 1021–1038.
Hasenaka, T., and I. S. E. Carmichael (1985), The cinder cones of Michoacán-Guanajuato, central Mexico: Their age, volume and distribution and magma discharge rate.
Heidbach, O., M. Tingay, A. Barth, J. Reinecker, D. Kurfeß, and B. Müller (2008), The world stress map database release 2008, WSM. Rel2008. [Available at http://www.world-stress-map.org/.]
Hippolyte, J. C., J. Angelier, and F. Roure (1994), A major geodynamic change revealed by Quaternary stress patterns in the Southern Apennines (Italy), *Tectonophysics*, *230*(3), 199–210.
IGM (1876), M. Vesuvio.
IGM (1906), Cono Vesuviano dopo l'eruzione dell'aprile 1906.
Iuliano, T., P. Mauriello, and D. Patella (2002), Looking inside Mount Vesuvius by potential fields integrated probability tomographies, *J. Volcanol. Geotherm. Res.*, *113*(3), 363–378.
Kyle, P. R., and J. W. Cole (1974), Structural control of volcanism in the McMurdo Volcanic Group, Antarctica, *Bull. Volcanol.*, *38*(1), 16–25.
Locardi, E., and R. Nicolich (1988), Geodinamica del Tirreno e dell'Appennino centro-meridionale: La nuova carta della Moho, *Mem. Soc. Geol. Ital.*, *41*, 121–140.
Marzocchi, W., and M. S. Bebbington (2012), Probabilistic eruption forecasting at short and long time scales, *Bull. Volcanol.*, *74*(8), 1777–1805.
Matthies, H. G. (2007), Quantifying uncertainty: Modern computational representation of probability and applications, in *Extreme Man-Made and Natural Hazards in Dynamics of Structures*, pp. 105–135, Springer, Dordrecht, Netherlands.
Mele, D., R. Sulpizio, P. Dellino, and L. La Volpe (2011), Stratigraphy and eruptive dynamics of a pulsating Plinian eruption of Somma-Vesuvius: The Pomici di Mercato (8900 years B.P.), *Bull. Volcanol.*, *73*(3), 257–278.
Milia, A., A. Raspini, and M. M. Torrente (2007), The dark nature of Somma-Vesuvius volcano: Evidence from the~3.5 ka B.P. Avellino eruption, *Quat. Int.*, *173*, 57–66.
Milia, A., M. M. Torrente, and F. Bellucci (2012), A possible link between faulting, cryptodomes and lateral collapses at Vesuvius volcano (Italy), *Global Planet. Change*, *90–91*, 121–134.
Mitchell, A. (1999), *The ESRI Guide to GIS Analysis: Geographic Patterns & Relationships*, vol. 1, 187 pp., ESRI, Inc., Redlands, Calif.
Muller, J. R., G. Ito, and S. J. Martel (2001), Effects of volcano loading on dike propagation in an elastic half-space, *J. Geophys. Res.*, *106*(B6), 11,101–11,113, doi:10.1029/2000JB900461.
Nazzaro, A. (1997), Il Vesuvio. Storia eruttiva e teorie vulcanologiche, Liguori editore, Napoli.
Neri, A., W. P. Aspinall, R. Cioni, A. Bertagnini, P. J. Baxter, G. Zuccaro, D. Andronico, S. Barsotti, P. D. Cole, and T. Esposti Ongaro (2008), Developing an event tree for probabilistic hazard and risk assessment at Vesuvius, *J. Volcanol. Geotherm. Res.*, *178*(3), 397–415.
Neri, A., A. Bevilacqua, T. Esposti Ongaro, R. Isaia, W. P. Aspinall, M. Bisson, F. Flandoli, P. J. Baxter, A. Bertagnini, and E. Iannuzzi (2015), Quantifying volcanic hazard at Campi Flegrei caldera (Italy) with uncertainty assessment: II. Pyroclastic density current invasion maps, *J. Geophys. Res. Solid Earth*, *120*, 2330–2349, doi:10.1002/2014JB011776.

Paoletti, V., S. Passaro, M. Fedi, C. Marino, S. Tamburrino, and G. Ventura (2016), Subcircular conduits and dikes offshore the Somma-Vesuvius volcano revealed by magnetic and seismic data, *Geophys. Res. Lett.*, *43*, 9544–9551, doi:10.1002/2016GL070271.

Porter, S. C. (1972), Distribution, morphology and size frequency of cinder cones on Mauna Kea volcano, Hawaii, *GSA Bull.*, *83*(12), 3607–3612.

Principe, C., J. C. Tanguy, S. Arrighi, A. Paiotti, M. Le Goff, and U. Zoppi (2004), Chronology of Vesuvius' activity from A.D. 79 to 1631 based on archeomagnetism of lavas and historical sources, *Bull. Volcanol.*, *66*(8), 703–724.

Principe, C., D. Giordano, M. Bisson, A. Paolillo, and R. Gianardi (2013), Volcanological map of the south-western sector of Vesuvius between Torre del Greco and Ercolano, SELCA Firenze.

Ricciardi, G. P. (2009), Diario del Monte Vesuvio: Venti secoli di immagini e cronache di un vulcano nella città, Edizioni scientifiche e artistiche, Napoli.

Rolandi, G., P. Petrosino, and J. Mc Geehin (1998), The interplinian activity at Somma–Vesuvius in the last 3500 years, *J. Volcanol. Geotherm. Res.*, *82*(1), 19–52.

Rosi, M., C. Principe, and R. Vecci (1993), The 1631 Vesuvius eruption. A reconstruction based on historical and stratigraphical data, *J. Volcanol. Geotherm. Res.*, *58*(1), 151–182.

Santacroce, R. (1987), *Somma-Vesuvius*, *Quad. Ric. Sci.*, 251 pp., CNR, Roma, Italy.

Santacroce, R., and A. Sbrana (2003), Geological map of Vesuvius, SELCA Firenze.

Santacroce, R., R. Cioni, P. Marianelli, A. Sbrana, R. Sulpizio, G. Zanchetta, D. J. Donahue, and J. L. Joron (2008), Age and whole rock-glass compositions of proximal pyroclastics from the major explosive eruptions of Somma-Vesuvius: A review as a tool for distal tephrostratigraphy, *J. Volcanol. Geotherm. Res.*, *177*(1), 1–18.

Santangelo, N., G. Ciampo, V. Di Donato, P. Esposito, P. Petrosino, P. Romano, E. R. Ermolli, A. Santo, F. Toscano, and I. Villa (2010), Late Quaternary buried lagoons in the northern Campania plain (southern Italy): Evolution of a coastal system under the influence of volcano-tectonics and eustatism, *Ital. J. Geosci.*, *129*(1), 156–175.

Scandone, R., L. Giacomelli, and P. Gasparini (1993), Mount Vesuvius: 2000 years of volcanological observations, *J. Volcanol. Geotherm. Res.*, *58*(1), 5–25.

Scandone, R., L. Giacomelli, and F. F. Speranza (2008), Persistent activity and violent strombolian eruptions at Vesuvius between 1631 and 1944, *J. Volcanol. Geotherm. Res.*, *170*(3–4), 167–180.

Scarpa, R., F. Tronca, F. Bianco, and E. Del Pezzo (2002), High resolution velocity structure beneath Mount Vesuvius from seismic array data, *Geophys. Res. Lett.*, *29*(21), 2040, doi:10.1029/2002GL015576.

Sparks, R. S. J., and W. P. Aspinall (2004), Volcanic activity: Frontiers and challenges in forecasting, prediction and risk assessment, in *The State of the Planet: Frontiers and Challenges in Geophysics*, edited by R. S. J. Sparks and C. J. Hawkesworth, pp. 359–373, AGU, Washington, D. C.

Sulpizio, R., D. Mele, P. Dellino, and L. La Volpe (2005), A complex, subplinian-type eruption from low-viscosity, phonolitic to tephri-phonolitic magma: The A.D. 472 (Pollena) eruption of Somma-Vesuvius, Italy, *Bull. Volcanol.*, *67*(8), 743–767.

Sulpizio, R., R. Cioni, M. A. Di Vito, R. Santacroce, A. Sbrana, and G. Zanchetta (2008), Comment on: "The dark nature of Somma-Vesuvius volcano: Evidence from the ~3.5 ka B.P. Avellino eruption" by Milia A., Raspini A., Torrente M. M., *Quat. Int.*, *192*(1), 102–109.

Tadini, A., et al. (2017), Assessing future vent opening locations at the Somma-Vesuvio volcanic complex: 2. Probability maps of the caldera for a future Plinian/sub-Plinian event with uncertainty quantification, *J. Geophys. Res. Solid Earth*, *122*, doi:10.1002/2016JB013860.

Tarquini, S., I. Isola, M. Favalli, F. Mazzarini, M. Bisson, M. T. Pareschi, and E. Boschi (2007), TINITALY/01: A new triangular irregular network of Italy, *Ann. Geophys.*, *50*(3).

Ventura, G., G. Vilardo and P. P. G. Bruno (1999), The role of flank failure in modifying the shallow plumbing system of volcanoes: an example from Somma-Vesuvius, Italy, *Geophys. Res. Lett.*, *26*(24), 3681–3684.

Ventura, G., G. Vilardo, G. Bronzino, G. Gabriele, R. Nappi, and C. Terranova (2005), Geomorphological map of the Somma-Vesuvius volcanic complex (Italy), *J. Maps*, *1*(1), 30–37.

Vilardo, G., G. Bronzino, and C. Terranova (2009), Sistema Informativo Sismotettonico della Regione Campania (SISCam 2.0), edited, Laboratorio di Geomatica e Cartografia, INGV-OV.

Vilardo, G., G. De Natale, G. Milano, and U. Coppa (1996), The seismicity of Mt. Vesuvius, *Tectonophysics*, *261*(1), 127–138.

Woo, G. (1999), *The Mathematics of Natural Catastrophes*, 292 pp., Imperial College Press, London.

Zollo, A., L. D'Auria, R. De Matteis, A. Herrero, J. Virieux, and P. Gasparini (2002), Bayesian estimation of 2-D P-velocity models from active seismic arrival time data: Imaging of the shallow structure of Mt Vesuvius (southern Italy), *Geophys. J. Int.*, *151*(2), 566–582.